Contents lists available at ScienceDirect

Lithos

journal homepage: www.elsevier.com/locate/lithos

Research Article

Petrogenesis of Late Jurassic two-mica granites and associated diorites and syenite porphyries in Guangzhou, SE China

Xiao Liu [a,b], Qiang Wang [a,b,c,*], Lin Ma [a,*], Zong-Yong Yang [a,d], Wan-Long Hu [a], Yi-Ming Ma [a,e], Jun Wang [a], Tong-Yu Huang [a]

[a] State Key Laboratory of Isotope Geochemistry, Guangzhou Institute of Geochemistry, Chinese Academy of Sciences, Guangzhou 510640, China
[b] College of Earth and Planetary Sciences, University of Chinese Academy of Sciences, Beijing, 100049, China
[c] CAS Center for Excellence in Tibetan Plateau Earth Sciences, Beijing 100101, China
[d] State Key Laboratory of Ore Deposit Geochemistry, Institute of Geochemistry, Chinese Academy of Sciences, Guiyang 550002, China
[e] School of Earth Sciences, China University of Geosciences, Wuhan 430074, China

A B S T R A C T

The South China Block (SCB) is considered to have undergone extensive reworking of continental crust. However, the mechanisms of this crustal reworking are unclear. Here, we report on Late Jurassic (162–155 Ma) two-mica granites and associated diorites and syenite porphyries from the Huolushan–Longyandong area of Guangzhou City, southeastern China. The two-mica granites have high SiO_2 contents (69.6–73.6 wt%) and weakly peraluminous to strongly peraluminous compositions. These rocks have enriched Sr–Nd–Hf isotopic compositions (($^{87}Sr/^{86}Sr$)$_i$ = 0.7094–0.7145; $\varepsilon_{Nd}(t)$ = −10.5 to −9.3; $\varepsilon_{Hf}(t)$ = −12.7 to −4.2). The Huolushan two-mica granites have variable zircon O isotopic compositions ($\delta^{18}O$ = 6.8‰–10.4‰), whereas the Longyandong two-mica granites have homogeneous compositions ($\delta^{18}O$ = 8.6‰–9.9‰). The Huolushan syenite porphyries have moderate SiO_2 (59.6–60.1 wt%) and high alkaline ($K_2O + Na_2O$ = 9.4–9.8 wt%) contents. Their Sr–Nd–Hf–O isotopic compositions (($^{87}Sr/^{86}Sr$)$_i$ = 0.7105–0.7119; $\varepsilon_{Nd}(t)$ = −9.9 to −9.8; $\varepsilon_{Hf}(t)$ = −14.1 to −5.9; $\delta^{18}O$ = 6.5‰–10.6‰) are similar to those of the Huolushan two-mica granites. The Huolushan diorites have moderate SiO_2 contents (59.9–60.4 wt%) and are high-K calc-alkaline and metaluminous with $Mg^\#$ values of 43.2–43.8. Their Sr—Nd isotopic compositions (($^{87}Sr/^{86}Sr$)$_i$ = 0.7106–0.7109, $\varepsilon_{Nd}(t)$ = −8.8 to −8.6) are less enriched than those of the two-mica granites and syenite porphyries. In addition, the diorites have high zircon $\delta^{18}O$ values (7.8‰–8.9‰) and a wide range of zircon $\varepsilon_{Hf}(t)$ values (−13.4 to −5.6). We propose that the Huolushan two-mica granites were derived from a metagreywacke-dominated hybridized source with minor juvenile crustal rocks and that the Longyandong two-mica granites were generated by partial melting of metagreywackes. The Huolushan syenite porphyries were formed by the mixing of metasedimentary-rock-derived felsic magmas and minor enriched-mantle-derived alkaline magmas. The Huolushan diorites were most likely derived by partial melting of mafic lower crust, with the dioritic magmas undergoing assimilation and fractional crystallization (AFC) during ascent. All of these intrusive rocks were likely formed in an extensional intraplate setting. The mantle-derived magmas, which could have been triggered by lithospheric extension, underplated the middle–lower crust and provided heat for crustal reworking and materials for late Mesozoic crustal growth.

© 2020 Elsevier B.V. All rights reserved.

1. Introduction

Reworking of continental crust involves repeated metamorphism, deformation, and magmatism of continental materials without a change in crustal- or lithospheric-scale volume (Holdsworth et al., 2001). The occurrence of continental crust reworking can be inferred on the basis of two main characteristics: (1) the stratigraphic ages of global sediments are younger than their Nd model ages, suggesting that sedimentary recycling has reworked former continental crust rocks (O'Nions et al., 1983); and (2) magmatic zircons in granitoids with elevated $\delta^{18}O$ (>8.0‰) and mantle $\delta^{18}O$ (5.3‰ ± 0.3‰) values are closely related to the reworking of recycled supracrustal sediments and infracrustal juvenile crust rocks, respectively (Zheng et al., 2007). Orogenic belts are divided into three types: collisional, accretionary, and intracratonic (Cawood et al., 2009). Intracratonic orogens are generally considered to be key regions for the reworking of continental crust (Shu et al.,

2015; Wang et al., 2013a, and references therein). The SCB is an important intracratonic orogen because it has a complex tectonic history and records multiple reworking events. After amalgamation of the Yangtze and Cathaysia blocks during the Neoproterozoic (no later than ca. 800 Ma; Li et al., 2009a; Wang et al., 2013b; Zhao, 2015; Shu et al., 2019), the SCB underwent continental crust reworking during the Neoproterozoic (Li et al., 2005, and references therein), early Paleozoic (Li et al., 2010; Shu et al., 2015; Wang et al., 2010, 2013a), early Mesozoic (Wang et al., 2007a, 2007b), and late Mesozoic (Li et al., 2007; Li et al., 2018; Li and Li, 2007; Zhou and Li, 2000). However, the mechanisms of crustal reworking in the SCB are debated.

Reworking of SCB continental crust during the Neoproterozoic was related to continental rifting caused by a mantle plume (Li et al., 2005, and references therein). Felsic rocks were derived by partial melting of crustal rocks heated by mantle-derived mafic magmas (Li et al., 2005, and references therein). Two mechanisms of SCB continental crust reworking during the early Paleozoic have been proposed: (1) early Paleozoic S-type granites were generated by the anatexis of middle- to upper-crustal rocks caused by large-scale doubly vergent thrusting triggered either by underthrusting or subduction of the hypothesized East China Sea Block and southeastern Yangtze Block continental crust beneath the Cathaysia Block (Shu et al., 2015); and (2) early Paleozoic I-type granites were formed by partial melting of lower-crustal rocks heated by mantle-derived mafic magmas during intracontinental orogenic collapse (Yu et al., 2016). Early Mesozoic reworking of SCB continental crust was related to intracontinental convergence during the assembly of Pangea, whereby the weaker SCB was squeezed between the stronger North China and Indochina blocks (Liu et al., 2018; Wang et al., 2007a; Wang et al., 2013a), or by flat subduction of the Paleo-Pacific plate (Li et al., 2007; Li and Li, 2007). Early Mesozoic S-type granites were formed by partial melting of middle- to upper-crustal rocks as a result of in situ radiogenic heating from the over-thickened crust (Wang et al., 2007b).

SCB continental crust underwent its most intense episode of reworking during the late Mesozoic (Jurassic and Cretaceous), forming a broad ~1300-km-wide intracontinental orogen (Li and Li, 2007) and generating extensive Mesozoic granitic magmatism and mineralization (Mao et al., 2013b; Zhou et al., 2006; Zhou and Li, 2000). Late Mesozoic continental reworking mechanisms can be summarized into two main types: those involving subduction of the Paleo-Pacific plate, and those associated with intraplate extension/rifting. Paleo-Pacific plate subduction models encompass NW–WNW-directed oblique subduction and subsequent roll-back of Paleo-Pacific oceanic lithosphere (Jiang et al., 2009, 2015; Zhou and Li, 2000), as well as flat slab subduction and subsequent slab foundering (Li et al., 2007; Li et al., 2018; Li and Li, 2007). In contrast, intraplate extension/rifting models describe the reactivation of pre-existing fault/rift systems (He et al., 2010; Zhou et al., 2006) and post-orogenic (Indosinian (Triassic): 252–201 Ma) lithospheric extension (Wang et al., 2013a; Zhao and Zheng, 2009). Intensive large-scale reworking of SCB continental crust during the late Mesozoic has been hypothesized to have required a heat supply from mantle-derived mafic magmas (Zhou and Li, 2000), although whether reworking of middle to upper crust could be induced by such a heating mechanism remains uncertain. It is also unclear whether reworking of SCB continental crust involved the addition of mantle-derived material (i.e., continental growth) (Li et al., 2009b; Zhao and Zheng, 2009).

In this study, we present detailed petrographic, geochronological, whole-rock major- and trace-elemental, and whole-rock Sr—Nd and zircon Hf—O isotopic data for two-mica granites and associated diorites and syenite porphyries in the Huolushan–Longyandong area of Guangzhou, Guangdong Province, southeastern China. These data are used to constrain the time of formation of the igneous rocks and to infer their petrogenesis and tectonic setting. The findings provide insights into continental crust reworking processes in the SCB during the late Mesozoic.

2. Geological background and sample descriptions

The SCB comprises the Yangtze Block in the northwest and the Cathaysia Block in the southeast, which were amalgamated during the Neoproterozoic along the Jiangshan–Shaoxing Fault (Li et al., 2009a; Wang et al., 2013b; Zhao, 2015; Shu et al., 2019; Fig. 1a–b). The basement of the Cathaysia Block is composed of Paleoproterozoic to early Neoproterozoic metamorphic rocks, covered by late Neoproterozoic to Paleozoic terrigenous and neritic marine sediments (Chen and Jahn, 1998, and references therein). The Paleoproterozoic basement is exposed mostly in southwestern Zhejiang Province (the Badu and Longquan groups) and northwestern Fujian Province (the Mayuan and Mamianshan groups) (Li et al., 1998). The Badu and Mayuan groups are composed primarily of biotite plagioclase granulites, mica–(quartz) schists, and minor amphibolites, whereas the Longquan and Mamianshan groups consist mainly of metamorphic volcanic–sedimentary rocks (Li et al., 1998). Zircon U—Pb ages of cores of inherited zircons from Badu Group metamorphic rocks suggest that the protoliths of the Badu Group formed predominantly at ca. 2.5 Ga (Yu et al., 2012). In addition, overgrowth rims of zircons from metamorphic rocks of the Badu Group show two episodes of granulite-facies metamorphism at 1.89–1.88 Ga and 252–234 Ma (Yu et al., 2012). Sm—Nd isotopic isochron and sensitive high-resolution ion microprobe zircon U—Pb dating of Mayuan Group granulites and amphibolites suggest a formation age for the Mayuan Group of 2.12–1.77 Ga (Li et al., 1998; Yuan et al., 1991). Mesoproterozoic to Neoproterozoic basement crops out mainly in central Jiangxi Province (Zhoutan Group) and consists of metasedimentary rocks and metabasalts (Jiang and Zhu, 2017, and references therein). Sm—Nd isotopic isochron dating of amphibolites indicates that the protoliths of the Zhoutan Group were generated at ca. 1.11 Ga (Jiang and Zhu, 2017, and references therein). The SCB was influenced by the early Paleozoic Caledonian orogeny between ca. 460 and 415 Ma, and by the early Mesozoic Indosinian orogeny between ca. 250 and 205 Ma (Wang et al., 2007b, 2013a). Widespread early Paleozoic and early Mesozoic granitoids were formed during these two orogenies (Wang et al., 2007b, 2013a).

The subsequent late Mesozoic Yanshanian (Jurassic– Cretaceous: 180–66 Ma) orogeny was characterized by magma flare-ups, and around 80% of SCB Mesozoic granitoids were formed during this period (Zhou et al., 2006). In particular, the Late Jurassic (ca. 160 Ma) is an important age peak for late Mesozoic granites (Huang et al., 2015a; Li et al., 2007; Li et al., 2018; Zhou et al., 2006). The ca. 160 Ma granites are distributed primarily in southern Hunan Province, central-southern Jiangxi Province, and the central and coastal parts of Guangdong Province (Huang et al., 2013, 2015a; Jiang et al., 2009; Jiang and Zhu, 2017; Li et al., 2007; Zhang et al., 2015; Zhou and Li, 2000) (Fig. 1b). In addition, minor ca. 160 Ma granites crop out in eastern Guangxi Province and the central and coastal areas of Fujian Province (Chen et al., 2017; Huang et al., 2015a; Wang et al., 2016a; Zhou and Li, 2000) (Fig. 1b). These granites are predominantly biotite bearing and commonly contain muscovite (Huang et al., 2015a; Jiang and Zhu, 2017). A few granitic intrusive rocks contain amphibole (Huang et al., 2013; Huang et al., 2015b; Jiang et al., 2009; Zhang et al., 2015, and references therein). Apart from the granitic magmatism, small but locally prominent outcrops of mafic rocks are found with these granites (He et al., 2010; Jiang et al., 2009; Li et al., 2004; Wang et al., 2003; Wu et al., 2020). Late Mesozoic magmatism has generally been linked to subduction of the Paleo-Pacific plate (Chu et al., 2019; Jiang et al., 2009, 2015; Li et al., 2007; Li et al., 2018; Li and Li, 2007; Zhou and Li, 2000).

Guangdong Province and its capital, Guangzhou City, are located in the southern Nanling Range in the Cathaysia Block (Fig. 1b, c). The Huolushan intrusive rocks comprise two-mica granites, diorites, and syenite porphyries, whereas the Longyandong intrusive rocks are composed of two-mica granites. The Huolushan syenite porphyries lie in the lower part of the field section, whereas the Huolushan two-mica granites are located in the upper part (Supplementary Fig. 1). The
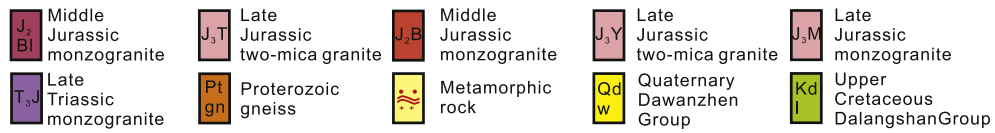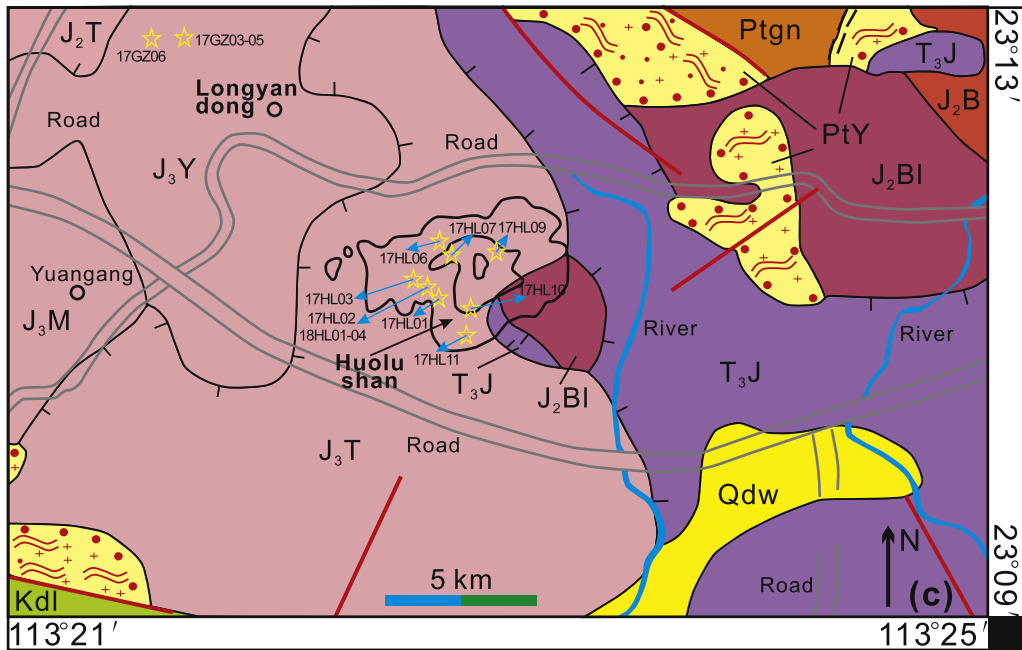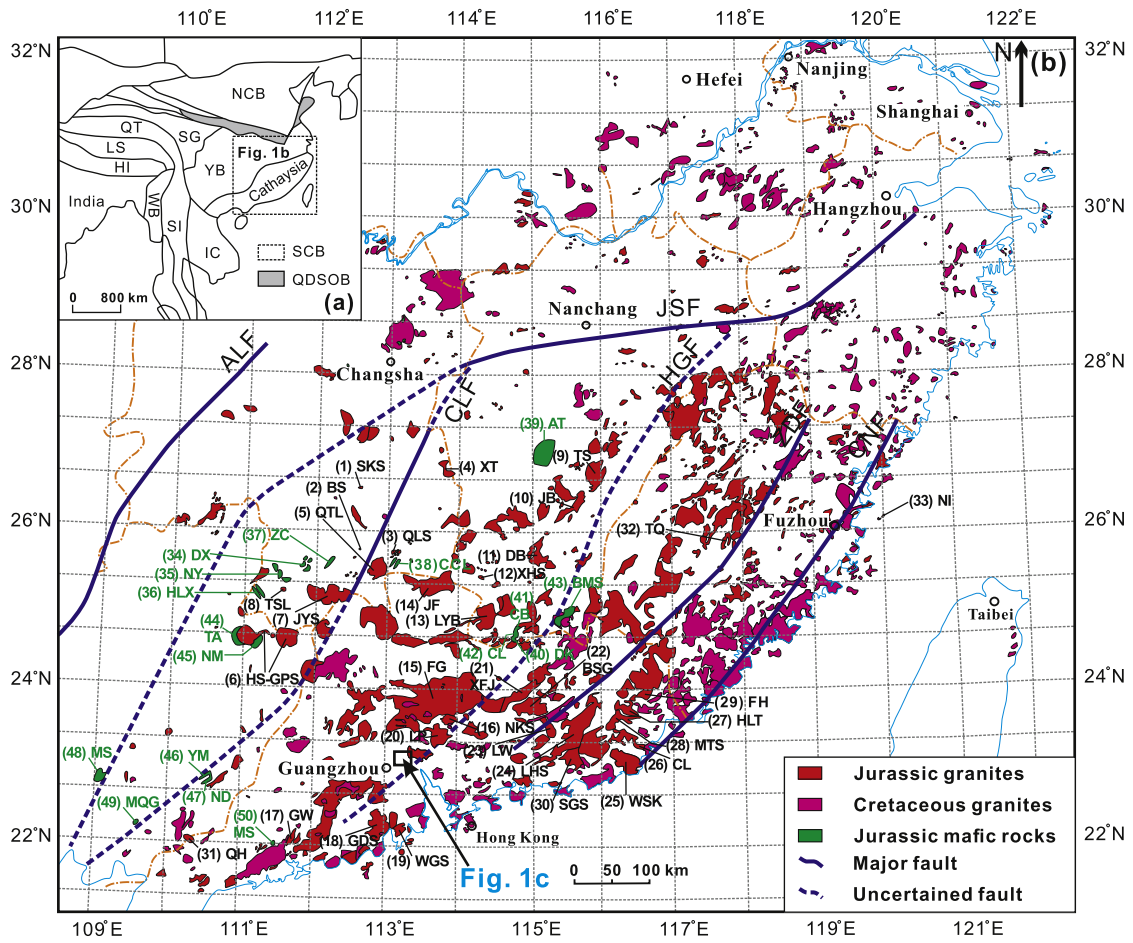
contact between syenite porphyries and two-mica granites is distinct (Supplementary Fig. 1a–b). The biotites of the Huolushan two-mica granites near the contact with granites and diorites (Supplementary Fig. 2a–b) show intense chloritization (Supplementary Fig. 2c–d). The granites are susceptible to weathering along joints and cracks (Guo et al., 2019). Abundant chlorite along the contact between granites and diorites suggests that the diorites intruded the granites along pre-existing fractures (Supplementary Fig. 2a–d). Locally, several oval mafic magmatic enclaves with sizes of a few centimeters are observed in the Huolushan two-mica granites (Supplementary Fig. 3a–c). Given that the diorites are younger than the granites, mafic magmatic enclaves within the granites were formed during an earlier magmatic stage than that of the diorites. Rounded shapes and fine-grained textures (Supplementary Fig. 3a–c) suggest that these mafic magmatic enclaves were formed by magma mixing (Vernon, 2004). Both the Huolushan and Longyandong intrusive rocks are intruded into Precambrian strata, and the Huolushan intrusive rocks are also intruded into Late Triassic granites (Fig. 1c).

The Huolushan two-mica granites are gray and typically have massive structure and inequigranular texture. They are composed of quartz (30–35 vol%), K-feldspar (25–30 vol%), plagioclase (15–20 vol%), biotite (5–10 vol%), and muscovite (5–8 vol%) with minor zircon, titanite, and Fe—Ti oxides (Fig. 2a, e–f). K-feldspar grains are larger than other mineral grains (Fig. 2a, f).

The Huolushan diorites are dark gray, massive, and fine grained. They are composed of plagioclase (35–40 vol%), amphibole (20–25 vol%), biotite (10–15 vol%), K-feldspar (5–10 vol%), and quartz (~5 vol%) with minor zircon, titanite, and Fe—Ti oxides (Fig. 2b, g–h).

The Huolushan syenite porphyries are dark gray, massive, and porphyritic, with phenocrysts of alkali-feldspar (20–25 vol%), albite plagioclase ($An_{0–5}$) (10–15 vol%), and amphibole (~5 vol%) (Fig. 2c, i–j). Most amphiboles have been chloritized and carbonatized by weathering. The matrix is composed of alkali-feldspar (35–40 vol%) and quartz (3–5 vol%) with minor zircon and titanite (Fig. 2i–j). In addition to supergene weathering, the syenite porphyries have been affected by hydrothermal alteration, as indicated by the presence of sericite (3 vol%) and pyrite (~3 vol%).

The Longyandong two-mica granites are gray, massive, and show a fine-grained granitic texture. They are composed of K-feldspar (25–30 vol%), quartz (30–35 vol%), plagioclase (10–15 vol%), biotite (5–10 vol%), and muscovite (5–8 vol%) with minor zircon and Fe—Ti oxides (Fig. 2d, k–l). Most biotites have been altered to chlorite and muscovite during supergene weathering.

3. Results

Analytical methods used during the study, including mineral composition analyses, zircon U—Pb age determinations, major- and trace-element analyses, Sr—Nd isotope analyses, and zircon O and Lu—Hf isotope analyses, are presented in the Supplementary Material.

3.1. Zircon U—Pb ages

SIMS (secondary ion mass spectrometer) zircon U—Pb dating results for the Huolushan two-mica granites, diorite, and syenite porphyry, as well as the Longyandong two-mica granite, are compiled in Supplementary Table 1 and presented in Fig. 3. Most zircon grains from the Huolushan two-mica granites, diorite, and syenite porphyry, and the Longyandong two-mica granite have sizes of 100–250 μm with aspect ratios of 2:1 to 4:1. Zircon grains from the Huolushan two-mica granites and syenite porphyry and the Longyandong two-mica granite display oscillatory zoning in cathodoluminescence (CL) images (Fig. 3a–c, e–f), whereas those from the Huolushan diorite show homogeneous textures (Fig. 3d). The clearly zoned or homogeneous textures and high Th/U ratios (0.07–1.68) of zircon grains from the Huolushan two-mica granites, diorite, and syenite porphyry, as well as the Longyandong two-mica granite, indicate a magmatic origin (Hoskin and Black, 2000).

SIMS zircon U—Pb dating of the Huolushan two-mica granite samples 17HL03-2, 17HL07-1, and 17HL09-1 yielded $^{206}Pb/^{238}U$ ages of 164–154 Ma, 165–157 Ma, and 164–157 Ma with weighted-mean ages of 158.4 ± 0.6 Ma (2σ; MSWD = 0.35; $n = 18$), 159.6 ± 1.8 Ma (2σ; MSWD = 0.07; $n = 14$), and 160.3 ± 1.3 Ma (2σ; MSWD = 1.4; $n = 13$), respectively. SIMS zircon U—Pb dating of the Huolushan diorite and syenite porphyry (samples 17HL03-1 and 18HL01-1) yielded $^{206}Pb/^{238}U$ ages of 158–152 Ma and 168–159 Ma with weighted-mean ages of 154.6 ± 0.5 Ma (2σ; MSWD = 0.33; $n = 20$) and 161.6 ± 1.6 Ma (2σ; MSWD = 0.12; $n = 13$), respectively (Fig. 3a–e; Supplementary Table 1). SIMS zircon U—Pb spot analyses of the Longyandong two-mica granite (sample 17GZ05–1) yielded $^{206}Pb/^{238}U$ ages of 164–155 Ma with a weighted-mean age of 159.1 ± 1.3 Ma (2σ; MSWD = 0.09; $n = 15$) (Fig. 3f; Supplementary Table 1). Therefore, the two-mica granites and associated diorites and syenite porphyries in the Huolushan–Longyandong area were formed during the Late Jurassic (162–155 Ma).

3.2. Mineral compositions

Mineral composition data for the Huolushan two-mica granites, diorites, and syenite porphyries and the Longyandong two-mica granites are given in Supplementary Tables 2–6. Plagioclases in the Huolushan two-mica granites are andesine and oligoclase ($An_{16–41}Ab_{57–82}Or_{1–3}$), whereas those in the Huolushan diorites and syenite porphyries are andesine with minor labradorite ($An_{31–64}Ab_{35–68}Or_{0–2}$) and albite ($An_{0–2}Ab_{97–100}Or_{0–1}$), respectively (Fig. 4a; Supplementary Table 2). Plagioclases in the Longyandong two-mica granites are oligoclase

Fig. 1. (a) Simplified regional map highlighting the major tectonic unites in eastern Asia (revised after Wang et al., 2005). SCB = South China Block; QDSOB = Qinling–Dabie–Sulu Orogenic Belt; NCB = North China Block; YB = Yangtze Block; IC = Indochina Block; SI = Sibumasu Block; SG = Songpan–Ganzi Accretionary Complex; WB = West Burma; Hi = Himalaya; LS = Lhasa; QT = Qiangtang. (b) Sketch map showing the location of Jurassic and Cretaceous granitic and Jurassic mafic rocks (modified from Sun, 2006). Fault abbreviations: CNF – Changle–Nanao Fault; ZDF – Zhenghe–Dabu Fault; HGF – Heyuan–Guangfeng Fault; CLF – Chenzhou–Linwu Fault; JSF – Jiangshan–Shaoxing Fault; ALF – Anhua–Luocheng Fault. Data sources for Late Jurassic (ca. 160 Ma) granites: Southern Hunan Province: (1) Shuikoushan (SKS, 158 Ma, Huang et al. (2015b) and references therein; (2) Baoshan (BS, 158 Ma), Huang et al. (2015b) and references therein; (3) Qianlishan (QLS, 163–153 Ma), Wang et al. (2016a) and references therein; (4) Xitian (XT, 154 Ma); (5) Qitianling (QTL, 163–153 Ma) and (6) Huashan–Guposhan (HS–GPS, 162 Ma), Wang et al. (2016a) and references therein; (7) Jiuyishan (or Jinjiling–Xishan) (JYS, 154 Ma), Huang et al. (2011); (8) Tongshanling (TSL, 164 Ma), Jiang et al. (2009). Southern Jiangxi Province: (9) Taoshan (TS, 154 Ma), (10) Jiangbei (JB, 159–157 Ma), and (11) Dabu (DB, 157 Ma), Jiang and Zhu (2017); (12) Xihuashan (XHS, 160–158 Ma), Huang et al. (2015a) and references therein; (13) Longyuanba (LYB, 157 Ma), Huang et al. (2015a) and references therein. Central and coastal areas of Guangdong Province: (14) Jiufeng (JF, 160–157 Ma), Huang et al. (2015a); (15) Fogang (FG, 165–159 Ma) and (16) Nankunshan (NKS, 158 Ma), Li et al. (2007); (17) Gangwei (GW, 166 Ma), (18) Gudoushan (GDS, 161 Ma), and (19) Wuguishan (WGS, 160 Ma), Huang et al. (2013); (20) Lapu (LP, 163 Ma), (21) Xinfengjiang (XFJ, 161 Ma), (22) Baishigang (BSG, 159 Ma), (23) Longwo (LW, 165 Ma), (24) Lianhuashan (LHS, 165 Ma), (25) Wushikeng (WSK, 160 Ma), (26) Chiliao (CL, 157 Ma), (27) Hulutian (HLT, 159 Ma), (28) Mantoushan (MTS, 164 Ma), (29) Fenghuang (FH, 161 Ma), and (30) Shigushan (SGS, 159 Ma), Zhang et al. (2015). Eastern Guangxi Province: (31) Qinghu (QH, 160 Ma), Li et al. (2009b). Central and coastal areas of Fujian Province: (32) Tangquan (TQ, 160 Ma), Wang et al. (2016a) and references therein; (33) Nankan Island (NI, 160 Ma), Chen et al. (2017). Data sources for Middle to Late Jurassic mafic rocks: (34) Daoxian (DX, 176–174 Ma), (35) Ningyuan (NY, 154–150 Ma), (36) Huilongxu (HLX, 172 Ma), (37) Zhicun (ZC, 146 Ma), (38) Changchengling (CCL, 178 Ma), (39) Antang (AT, 168 Ma), (40) Dongkeng (DK, 178 Ma), (41) Chebu (CB, 176–173 Ma), (42) Chenglong (CL, 182 Ma), (43) Baimianshan (BMS, 173 Ma), (44) Tong'an (TA, 163 Ma), (45) Niumiao (NM, 161 Ma), (46) Yangmei (YM, 162 Ma), (47) Nandu (ND, 160 Ma), (48) Mashan (MS, 160 Ma), (49) Maqigang (MQG, 160 Ma), (50) Ma–Shan (MS, 164 Ma), Wang et al. (2003), Li et al. (2004), and He et al. (2010). (c) Simplified geological map of the Huolushan and Longyandong intrusive rocks (modified after Guangzhou Geological Maps at a scale of 1:250,000 (GDGBMR, 1988)), showing rock types and sample locations.
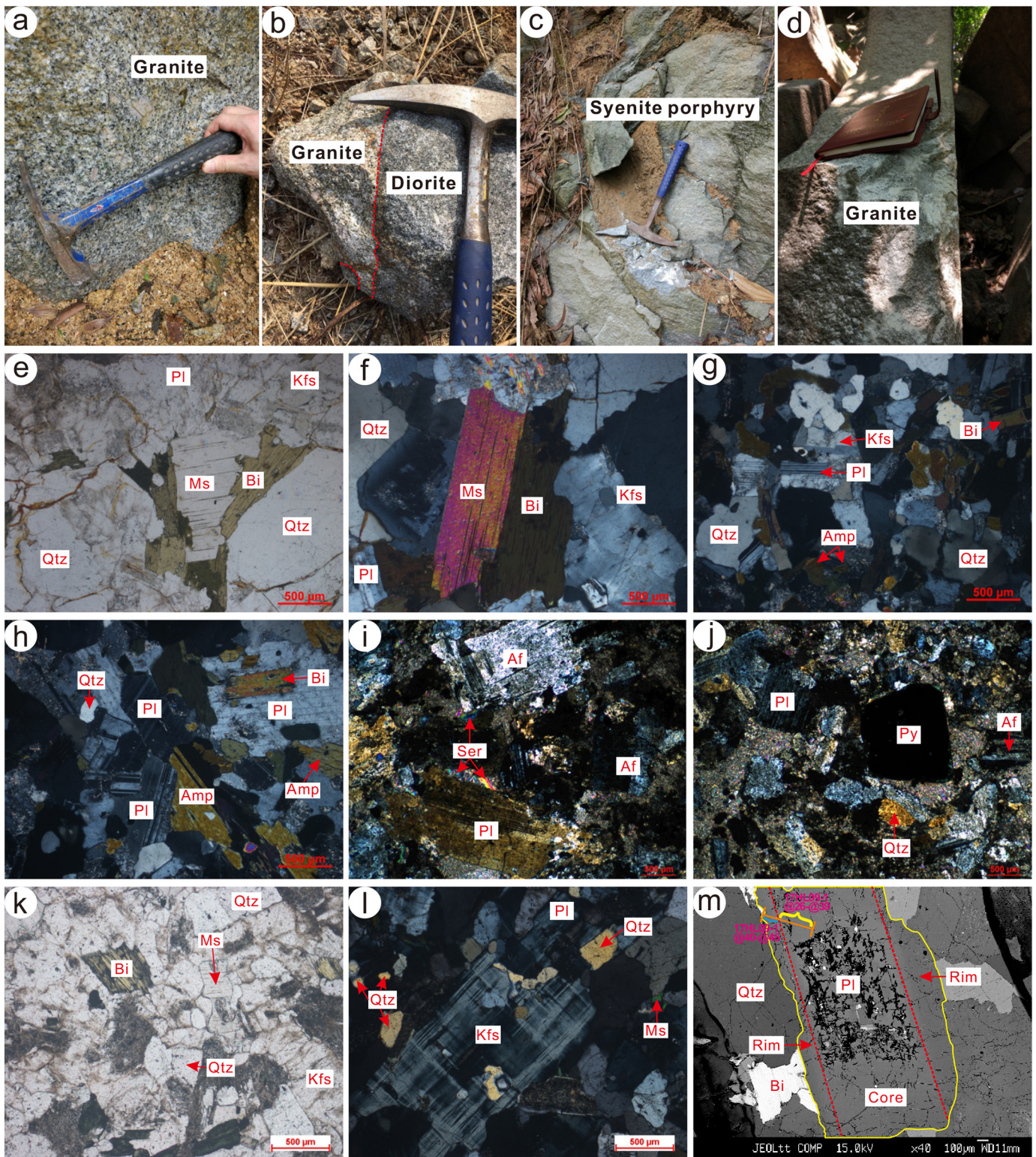
Fig. 2. Field photographs (a–d), plane-polarized-light photomicrographs (e and k), cross-polarized-light photomicrographs (f–j and l), and backscattered electron image (m) of the Huolushan two-mica granites, diorites, and syenite porphyries and the Longyandong two-mica granites: (a, e, f, and m) Huolushan two-mica granites; (b, g, and h) Huolushan diorites; (c, i, and j) Huolushan syenite porphyries; (d, k, and l) Longyandong two-mica granites. Mineral abbreviations: Pl – plagioclase; Kfs – potassium feldspar; Bi – biotite; Ms. – muscovite; Qtz – quartz; Amp – amphibole; Af – alkali-feldspar; Ser – sericite; Py – pyrite.

$(An_{10–23}Ab_{76–89}Or_{0–1})$ (Fig. 4a; Supplementary Table 2). K-feldspars in the Huolushan two-mica granites $(An_{0–0.3}Ab_{7–17}Or_{82–93})$ and diorites $(An_{0.2–0.3}Ab_{9–10}Or_{90–91})$, and in the Longyandong two-mica granites $(An_{0–0.5}Ab_{3–13}Or_{87–97})$ are all sanidine (Fig. 4a; Supplementary

Table 3). Biotites in the Huolushan and Longyandong two-mica granites are classified as lepidomelane with moderate MgO (5.1–7.2 wt%) and TiO_2 (1.7–2.9 wt%) contents, whereas biotites from the Huolushan diorites are magnesian biotites with high MgO (10.9–12.7 wt%) and
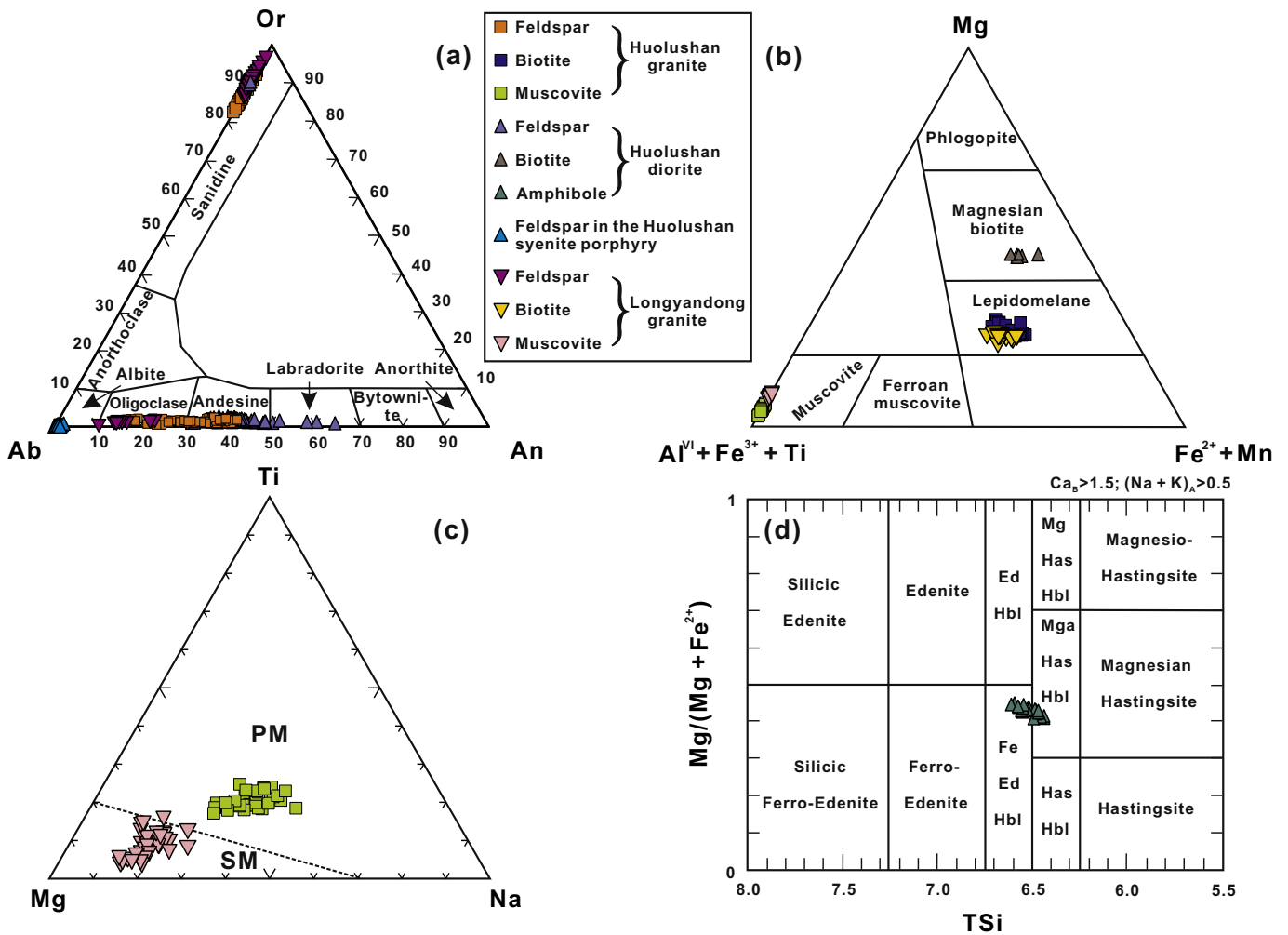
Fig. 3. SIMS zircon U—Pb concordia diagrams and cathodoluminescence (CL) images of zircons: (a)–17HL07-1 (Huolushan granite); (b)–17HL09-1 (Huolushan granite); (c)–17HL03-2 (Huolushan granite); (d)–17HL03-1 (Huolushan diorite); (e)–18HL01-1 (Huolushan syenite porphyry); (f)–17GZ05-1 (Longyandong granite). The fuchsia, yellow, and orange circles on CL images of zircons represent SIMS age points, O isotope points, and LA–ICP–MS (laser ablation ion coupled plasma mass spectrometry) Hf isotope points, respectively. The fuchsia, yellow, and orange numbers next to the corresponding circles represent age results, $\delta^{18}O$ values, and $\varepsilon_{Hf}(t)$ values of zircons, respectively.

Fig. 4. Chemical characteristics of minerals for the Huolushan two-mica granites, diorites, and syenite porphyries and the Longyandong two-mica granites. (a) Ab–Or–An diagram for feldspars (Ab – Albite, Or – Potassium feldspar, An – Anorthite); (b) Mica compositions in a triangular Mg–Al^{VI} + Fe^{3+} + Ti–Fe^{2+} + Mn diagram; (c) Muscovite Mg–Ti–Na diagram (Miller et al., 1981) (PM = primary muscovite, SM = secondary muscovite); (d) Classification diagram for calcic group amphiboles (Hawthorne, 1981).

moderate TiO$_2$ (1.5–3.3 wt%) contents (Fig. 4b; Supplementary Table 4). Muscovites in the Huolushan two-mica granites are primary, whereas those in the Longyandong two-mica granites are secondary, as shown by their higher MgO (1.3–1.9 wt% and 0.6–1.3 wt%, respectively) and lower TiO$_2$ (0.1–0.8 wt% and 0.2–1.2 wt%, respectively) and Na$_2$O (0.2–0.5 wt% and 0.4–0.7 wt%, respectively) contents compared with the former (Fig. 4c; Supplementary Table 5). Amphiboles in the Huolushan diorites are classified as ferro-edenitic hornblende and magnesio-hastingsitic hornblende (Mg$^{\#}$ = 41–45) (Mg$^{\#}$ = 100 × Mg^{2+}/[Mg^{2+} + Fe^{2+}]) following the nomenclature of Hawthorne (1981) (Fig. 4d; Supplementary Table 6).

3.3. Whole-rock major and trace elements

3.3.1. Huolushan two-mica granites, diorites, and syenite porphyries

Whole-rock major- and trace-element data for the Huolushan two-mica granites, diorites, and syenite porphyries and the Longyandong two-mica granites are given in Supplementary Table 7. The Huolushan two-mica granites have high SiO$_2$ (69.6–73.6 wt%), K$_2$O (4.8–5.8 wt%), and Na$_2$O (2.8–3.3 wt%) contents, with K$_2$O > Na$_2$O, and plot in the shoshonitic or subalkalic fields in discrimination diagrams (Fig. 5a–b, d; Supplementary Table 7). Their A/CNK (molar Al$_2$O$_3$/[CaO + Na$_2$O + K$_2$O]) values range from 1.04 to 1.12 and plot in the

peraluminous field (Fig. 5c). The Huolushan diorites have SiO$_2$ and MgO contents of 59.9–60.4 wt% and 2.86–2.90 wt%, respectively. They are high-K calc-alkaline and metaluminous (A/CNK = 0.87) with low Mg$^{\#}$ (molar MgO/[molar MgO + molar FeO^T] × 100) values of 43.2–43.8 (Fig. 5a–c; Supplementary Table 7). The Huolushan syenite porphyries have moderate SiO$_2$ (59.6–60.1 wt%) and high K$_2$O (4.6–5.1 wt%) and Na$_2$O (4.7–4.8 wt%) contents, and plot in the shoshonitic or alkalic fields diagrams of Na$_2$O + K$_2$O, K$_2$O, and Na$_2$O + K$_2$O – CaO versus SiO$_2$ diagrams (Fig. 5a–b, d; Supplementary Table 7). The A/CNK values of these rocks lie between 0.98 and 1.13 and plot in the metaluminous or peraluminous fields in an A/CNK versus A/NK diagram (Fig. 5c). The Huolushan two-mica granites have lower Al$_2$O$_3$, TiO$_2$, Fe$_2$O$_3^T$, CaO, P$_2$O$_5$, and MgO contents, higher K$_2$O contents, and similar Na$_2$O contents compared with the diorites (Supplementary Fig. 4a–c, e, g–h). In addition, the Huolushan two-mica granites exhibit lower Al$_2$O$_3$, TiO$_2$, Fe$_2$O$_3^T$, CaO, Na$_2$O, and P$_2$O$_5$ contents (Supplementary Fig. 4a–c, e, f–g) but similar K$_2$O and MgO contents compared with the syenite porphyries (Supplementary Fig. 4d, h).

The Huolushan two-mica granites and syenite porphyries show enrichment in light rare-earth elements (LREEs), moderately fractionated REE patterns ((La/Yb)$_{CN}$ = 11.0–21.8, where "CN" denotes chondrite-normalized), and pronounced negative Eu anomalies (Eu/Eu* = Eu$_{CN}$/(Sm$_{CN}$ × Gd$_{CN}$)$^{1/2}$) of 0.30–0.39 in chondrite-normalized element-
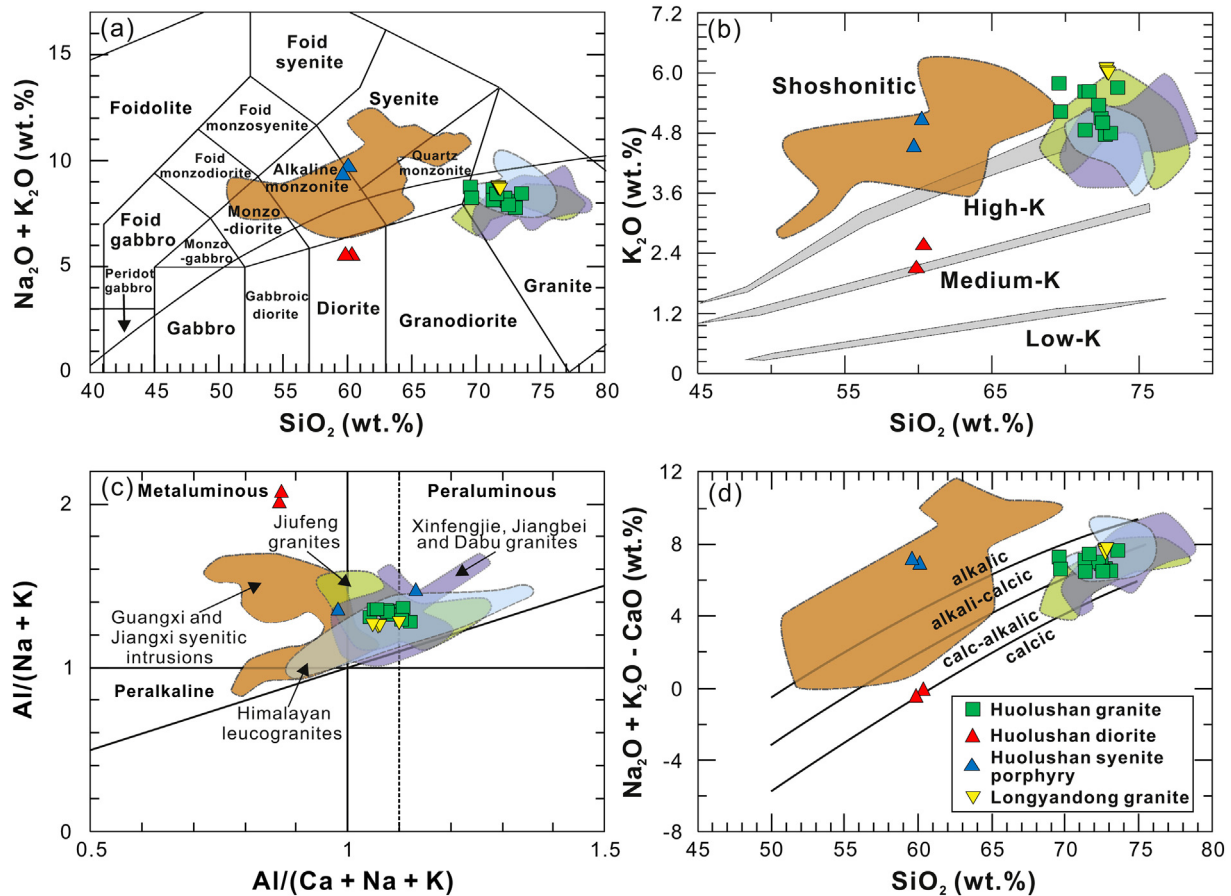
Fig. 5. Major-element classification diagrams for the Huolushan two-mica granites, diorites, and syenite porphyries and the Longyandong two-mica granites: (a) TAS diagram; (b) K_2O versus SiO_2 diagram; (c) A/NK versus A/CNK diagram; (d) ($Na_2O + K_2O — CaO$) versus SiO_2 diagram. Data for Jurassic Jiufeng granites, Jurassic Xinfengjie, Jiangbei, and Dabu granites, Jurassic Guangxi and Jiangxi syenitic intrusions in the SCB, and Himalayan leucogranites are from Li et al. (2004), He et al. (2010), Guo and Wilson (2012), Huang et al. (2015a), and Jiang and Zhu (2017) respectively.

variation diagrams (Fig. 6a, c). In primitive-mantle (PM)-normalized element-variation diagrams, the Huolushan two-mica granites and syenite porphyries display enrichment in Rb, Th, U, and Pb and show negative Ba, Sr, Nb, and Ti anomalies (Fig. 6b, d). The Huolushan diorites are characterized by slightly enriched LREE patterns ($(La/Yb)_{CN}$ = 9.4–9.8) with weak negative Eu anomalies (Eu/Eu^* = 0.62–0.63) in a chondrite-normalized diagram (Fig. 6c). In addition, they exhibit slight enrichment in Rb, Th, U, and Pb, and negative Ba, Sr, Nb, Ta, and Ti anomalies in a PM-normalized element-variation diagram (Fig. 6d).

3.3.2. Longyandong two-mica granites

The Longyandong two-mica granites have high SiO_2 (72.7–72.9 wt%), K_2O (6.0–6.1 wt%), and Na_2O (2.6–2.7 wt%) contents, with $K_2O > Na_2O$, and plot in the shoshonitic or subalkalic fields (Fig. 5a–b, d; Supplementary Table 7). Their A/CNK values range from 1.05 to 1.10 and plot in the peraluminous field (Fig. 5c). Compared with the Huolushan two-mica granites, the Longyandong two-mica granites overall have lower Al_2O_3, TiO_2, $Fe_2O_3^T$, CaO, Na_2O, P_2O_5, and MgO contents (Supplementary Fig. 4a–c, e–h), and higher K_2O contents (Supplementary Fig. 4d). The Longyandong two-mica granites have high total REE ($\sum$REE) contents (452–809 ppm; Supplementary Table 7) with moderately enriched LREE patterns ($(La/Yb)_{CN}$ = 16.0–22.0) and pronounced negative Eu anomalies (Eu/Eu^* = 0.27–0.29) (Fig. 6a). They are enriched in Rb, Th, U, and Pb, and depleted in Ba, Sr, Nb, Ta, and Ti in a PM-normalized element-variation diagram (Fig. 6b).

3.4. Sr–Nd–Hf–O isotopic compositions

3.4.1. Huolushan two-mica granites, diorites, and syenite porphyries

Whole-rock Sr—Nd and zircon Hf—O isotope data for the Huolushan two-mica granites, diorites, and syenite porphyries and the Longyandong two-mica granites are given in Supplementary Tables 8–9. According to the obtained SIMS zircon U—Pb ages, initial Sr–Nd–Hf isotopic ratios were calculated at 160 Ma for the Huolushan two-mica granites and syenite porphyries as well as the Longyandong two-mica granites and at 155 Ma for the Huolushan diorites. The Huolushan two-mica granites and syenite porphyries both have variable initial $^{87}Sr/^{86}Sr$ ratios (0.7130–0.7145 and 0.7105–0.7119, respectively), initial $^{176}Hf/^{177}Hf$ ratios (0.2823–0.2826 and 0.2823–0.2825, respectively), $\varepsilon_{Hf}(t)$ values (−12.7 to −4.2 and −14.1 to −5.9, respectively), and $\delta^{18}O$ values (6.8‰–10.4‰ and 6.5‰–10.6‰, respectively), and uniform $\varepsilon_{Nd}(t)$ values (−10.5 to −10.2 and −9.9 to −9.8, respectively) (Fig. 7a–b; Supplementary Figs. 5a, c–e and 6a, c–e; Supplementary Tables 8–9). The Huolushan diorites have relatively homogeneous initial $^{87}Sr/^{86}Sr$ ratios (0.7106–0.7109), $\varepsilon_{Nd}(t)$ values (−8.8 to −8.6), and $\delta^{18}O$ values (7.8‰–8.9‰), and variable initial $^{176}Hf/^{177}Hf$ ratios (0.2823–0.2825) and $\varepsilon_{Hf}(t)$ values (−13.4 to −5.6) (Fig. 7a–b; Supplementary Figs. 5b and 6b; Supplementary Tables 8–9).

3.4.2. Longyandong two-mica granites

The Longyandong two-mica granites have uniform initial $^{87}Sr/^{86}Sr$ ratios (0.7094–0.7095), $\varepsilon_{Nd}(t)$ values (−9.4 to −9.3), and $\delta^{18}O$ values (8.6‰–9.9‰), and variable initial $^{176}Hf/^{177}Hf$ ratios (0.2823–0.2825)
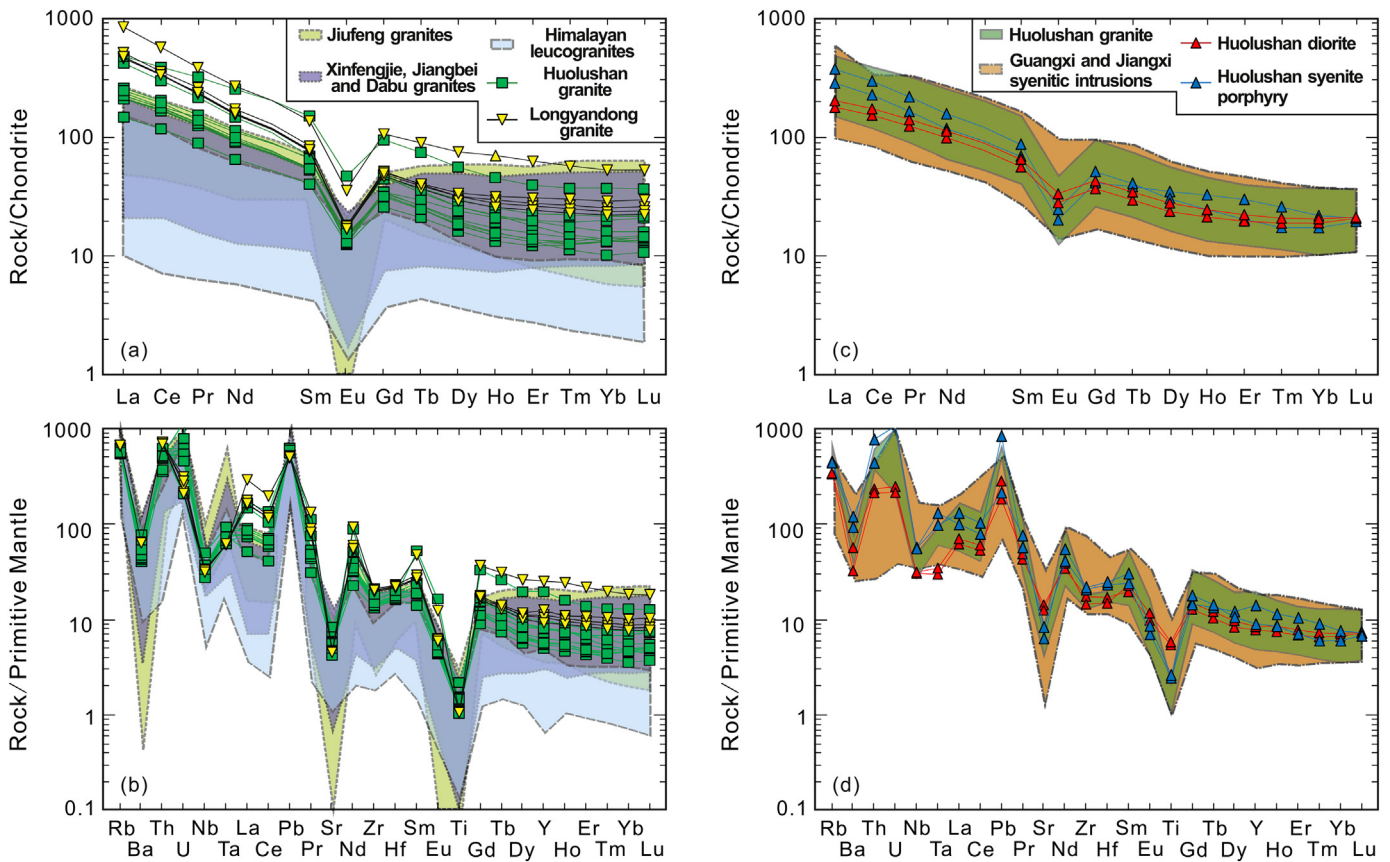
Fig. 6. (a) Chondrite-normalized REE patterns for the Huolushan two-mica granites and the Longyandong two-mica granites; (b) Primitive-mantle-normalized multi-element diagram for the Huolushan two-mica granites and the Longyandong two-mica granites; (c) Chondrite-normalized REE patterns for the Huolushan syenite porphyries and diorites; (d) Primitive-mantle-normalized multi-element diagram for the Huolushan syenite porphyries and diorites. Normalizing values are after Sun and McDonough (1989). Data sources are the same as in Fig. 5.

4. Discussion

4.1. Huolushan two-mica granites

4.1.1. Hybridized magma source

The Huolushan two-mica granites exhibit similar major- and trace-element characteristics to those of the sedimentary-rock-derived Himalayan leucogranites (Guo and Wilson, 2012), Late Jurassic Jiufeng two-mica granites (northern Guangdong Province) (Huang et al., 2015a), and Late Jurassic Xinfengjie, Jiangbei, and Dabu (central-southern Jiangxi Province) biotite granites and muscovite-bearing granites (Jiang and Zhu, 2017; Figs. 5 and 6) of the SCB. In particular, the Th contents (29.8–52.6 ppm) and Th/La ratios (0.41–0.88) of the Huolushan two-mica granites are similar to those of the above-mentioned sedimentary-rock-derived granites (1.35–46.3 ppm and 0.23–3.00, respectively) (Supplementary Table 7). Furthermore, the Huolushan two-mica granites have similar Nd isotopic compositions ($\varepsilon_{Nd}(t) = -10.5$ to -10.2; Fig. 7a; Supplementary Table 8) to Cathaysia Block basement metasedimentary rocks as well as Jiangxi Province Jurassic S-type granites ($\varepsilon_{Nd}(t) = -12.9$ to -9.2, Yuan et al., 1991; Shen et al., 1999; Jiang and Zhu, 2017) and Triassic Darongshan (eastern Guangxi Province) cordierite-bearing granites ($\varepsilon_{Nd}(t) = -13.0$ to -9.9, Qi et al., 2007) in the SCB, and Himalayan leucogranites ($\varepsilon_{Nd}(t) = -13.3$ to -11.5, Huang et al., 2017; Fig. 7a). They also have more enriched Sr—Nd isotopic compositions (($^{87}Sr/^{86}Sr)_i = 0.7106$–0.7109; $\varepsilon_{Nd}(t) = -10.5$ to -10.2) than the Fogang (central

Guangdong Province) I-type granites (($^{87}Sr/^{86}Sr)_i = 0.7098$–0.7136; $\varepsilon_{Nd}(t) = -12.2$ to -4.3; Li et al., 2007; Fig. 7a; Supplementary Table 8). Moreover, most zircons from the Huolushan two-mica granites have high $\delta^{18}O$ values (8.0‰–10.4‰; Supplementary Fig. 6a, c–d; Supplementary Table 9) that are similar to those of zircons from sedimentary-rock-derived Himalayan leucogranites, Neoproterozoic Jiuling S-type granites, Triassic Darongshan cordierite-bearing granites, and Jurassic Jiuyishan A-type granites ($\delta^{18}O = 8.2‰$–12.9‰; Fig. 8) in the SCB. Experimental data for common crustal melts have been summarized by Altherr et al. (2000) and Altherr and Siebel (2002). According to those data, the Huolushan two-mica granites with their moderate molar CaO/(MgO + FeO^T) and high molar Al$_2$O$_3$/(MgO + FeO^T) ratios are consistent with a metagreywacke source (Fig. 9).

However, experimental studies have suggested that partial melts of metasedimentary rocks (metagreywackes and metapelites) are all strongly peraluminous (A/CNK > 1.1) (Patiño Douce and Harris, 1998), which is inconsistent with the Huolushan two-mica granites, which are weakly to strongly peraluminous (A/CNK = 1.04–1.12; Fig. 5c). Also, the Huolushan two-mica granites overall have more depleted zircon Hf isotopic compositions ($\varepsilon_{Hf}(t) = -12.7$ to -4.2; Fig. 7b; Supplementary Table 9) than the Triassic Luxi, Xiazhuang, and Fucheng (southeastern Jiangxi Province) S-type granites ($\varepsilon_{Hf}(t) = -12.2$ to -5.8; Gao et al., 2014) and the Jurassic Jiufeng, Xinfengjie, Jiangbei, and Dabu S-type granites ($\varepsilon_{Hf}(t) = -17.7$ to -6.3; Huang et al., 2015a; Jiang and Zhu, 2017) in the SCB. In addition, several zircon grains from the Huolushan granites have lower $\delta^{18}O$ values (6.8‰–7.9‰; Supplementary Fig. 6a, c–d; Supplementary Table 9) than the above-mentioned sedimentary-rock-derived granites (Fig. 8). The negative relationship between zircon $\varepsilon_{Hf}(t)$ and $\delta^{18}O$ (Fig. 8) indicates that

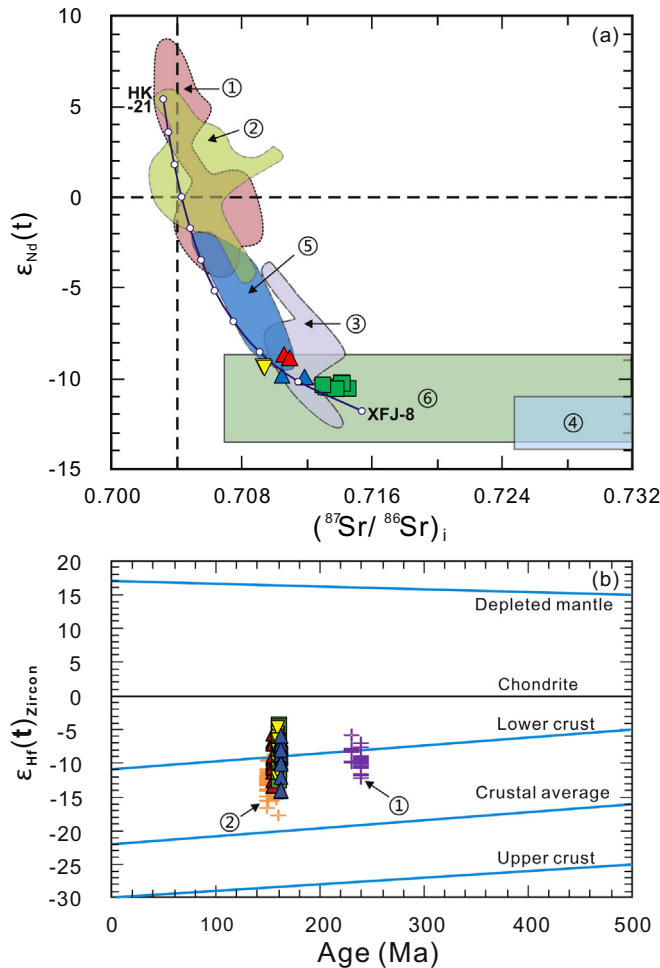summary, the source materials of the Huolushan two-mica granites were dominated by metagreywackes with minor juvenile crustal rocks.

The Huolushan two-mica granites were probably derived by partial melting of metagreywackes, driven by the fluid-absent mica breakdown reaction. K_2O contents (4.8–5.8 wt%) of the Huolushan two-mica granites are higher than their Na_2O (2.8–3.3 wt%) contents (Supplementary Table 7). In addition, the Huolushan two-mica granites have high zircon and monazite saturation temperatures (T_{Zr} = 781–809 °C and T_{LREE} = 753–861 °C, respectively; Fig. 10a–b), which argues against water-saturated melting of plagioclase at low temperatures (~650 °C; Huang et al., 2015a, and references therein). Moreover, the overall negative trend observed in an Rb/Sr versus Ba diagram (Supplementary Fig. 7a) for the Huolushan granites also supports mica dehydration melting (Gao and Zeng, 2014).

The magma that formed the Huolushan two-mica granites may have originated from a depth of 16.5–20.0 km (middle crust), based on the following lines of evidence. La/Yb and Sr/Y ratios of felsic rocks intrinsically reflect the presence of mineral assemblages in the magma source region (Tang et al., 2017, and references therein). The relatively high La/Yb and low Sr/Y ratios of the Huolushan granites suggest that both plagioclase and garnet were residual mineral phases during magma generation (Supplementary Fig. 7b; Wang et al., 2016b). Given that garnet can be stable to pressures as low as 5 kbar (corresponding to a crustal depth of 16.5 km) during fluid-absent melting of metasedimentary rocks (Patiño Douce and Harris, 1998), the magma origin depth of the Huolushan granites is >16.5 km. In addition, primary muscovites can be used to constrain the temperatures and pressures of peraluminous magmas (Huang et al., 2015a, and references therein). Low (FeO^T + MgO) contents are consistent with a low celadonite component in the high-Ti (>0.4 wt%) primary muscovites from the Huolushan two-mica granites (Supplementary Table 5), suggesting that they crystallized at high temperatures (Miller et al., 1981). The Si-in-muscovite barometer (Huang et al., 2015a; Tang et al., 2017, and references therein) gives a pressure of 6.0 ± 0.5 (1SD) kbar (~20 km)
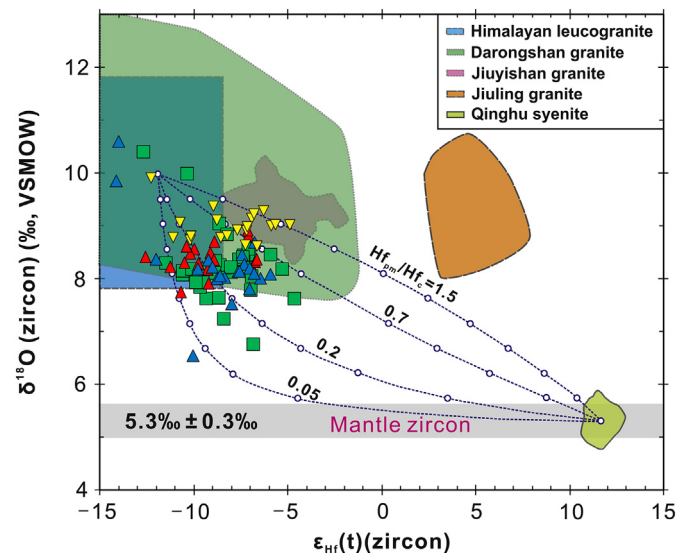
Fig. 7. (a) $\varepsilon_{Nd}(t)$ versus ($^{87}Sr/^{86}Sr)_i$ diagram for the Huolushan two-mica granites, diorites, and syenite porphyries and the Longyandong two-mica granites. Data for Middle Jurassic within-plate basalts and gabbros of the Cathaysia Block (①) are from Li et al. (2003) and Wang et al. (2003); data for Jurassic Guangxi and Jiangxi Province syenitic intrusions in the SCB (②) are from Li et al. (2004) and He et al. (2010); data for Fogang granites (③) are from Li et al. (2007); data for Himalayan leucogranites (④) are from Huang et al. (2017); data for lower-crust granulite xenoliths of the Cathaysia Block (⑤) are from Yu et al. (2003); data for basement metasedimentary rocks and Jurassic S-type granites of the Cathaysia Block (⑥) are from Yuan et al. (1991), Shen et al. (1999), and Jiang and Zhu (2017). The mixing end-members are: Guangxi Province Jurassic Qinghu syenites from the SCB (HK-21: $\varepsilon_{Nd}(t)$ = + 5.45, ($^{87}Sr/^{86}Sr)_i$ = 0.7032, Nd = 39.9 ppm, and Sr = 678 ppm) from Li et al. (2004); and Jurassic S-type granites from Jiangxi Province of the SCB (XFJ-8: $\varepsilon_{Nd}(t)$ = −11.8, ($^{87}Sr/^{86}Sr)_i$ = 0.7153, Nd = 42 ppm, and Sr = 158 ppm) from Jiang and Zhu (2017). Initial Sr—Nd isotopic compositions of lower-crust granulite xenoliths, basement metasedimentary rocks, and Mesozoic S-type granites of the Cathaysia Block are recalculated to 160 Ma. (b) Zircon $\varepsilon_{Hf}(t)$ versus age diagram for the Huolushan two-mica granites, diorites, and syenite porphyries and the Longyandong two-mica granites. Data for Triassic S-type granites in the SCB (①) are from Gao et al. (2014); data for Jurassic S-type granites in the SCB (②) are from Huang et al. (2015a) and Jiang and Zhu (2017). The legend for (a) and (b) is the same as in Fig. 5.

metaluminous juvenile crustal rocks or mantle-derived mafic magmas with depleted Hf isotopic compositions and low $\delta^{18}O$ values were involved in the source material of the Huolushan two-mica granites. A simple zircon Hf—O isotope mixing model shows that the Huolushan two-mica granites might contain 40%–50% of PM-derived material (Fig. 8). However, this is inconsistent with the radiogenic initial $^{87}Sr/^{86}Sr$ (>0.7098) and unradiogenic whole-rock Nd isotopes (ε_{Nd} (t) = −10.5 to −10.2) of the Huolushan two-mica granites. Furthermore, Mg# values (25–33; Supplementary Table 7) of the Huolushan two-mica granites fall within the field of crustal melts (Fig. 9c). Therefore, we suggest that other juvenile crustal rocks were involved in the metagreywacke source of the Huolushan two-mica granites. In

Fig. 8. Zircon Hf versus O isotopic compositions of the Huolushan two-mica granites, diorites, and syenite porphyries and the Longyandong two-mica granites (modified from Li et al., 2009b). The legend is the same as in Fig. 5. Data for Qinghu syenites are from Li et al. (2009b), for Jiuyishan granites are from Huang et al. (2011), for Darongshan granites are from Jiao et al. (2015), for Jiuling granites are from Rong et al. (2017), and for Himalayan leucogranites are from Hopkinson et al. (2017). The dashed lines denote two-component mixing trends between mantle- and supracrustal-derived magmas. Hf_{pm}/Hf_c is the ratio of Hf concentration in the parental mantle magma (pm) to that in crustal melt (c) for each curve, and the small open circles represent 10% mixing increments assuming that mantle zircon has ε_{Hf} = +12 and $\delta^{18}O$ = 5.6‰ and that supracrustal zircon has ε_{Hf} = −12 and $\delta^{18}O$ = 10‰.
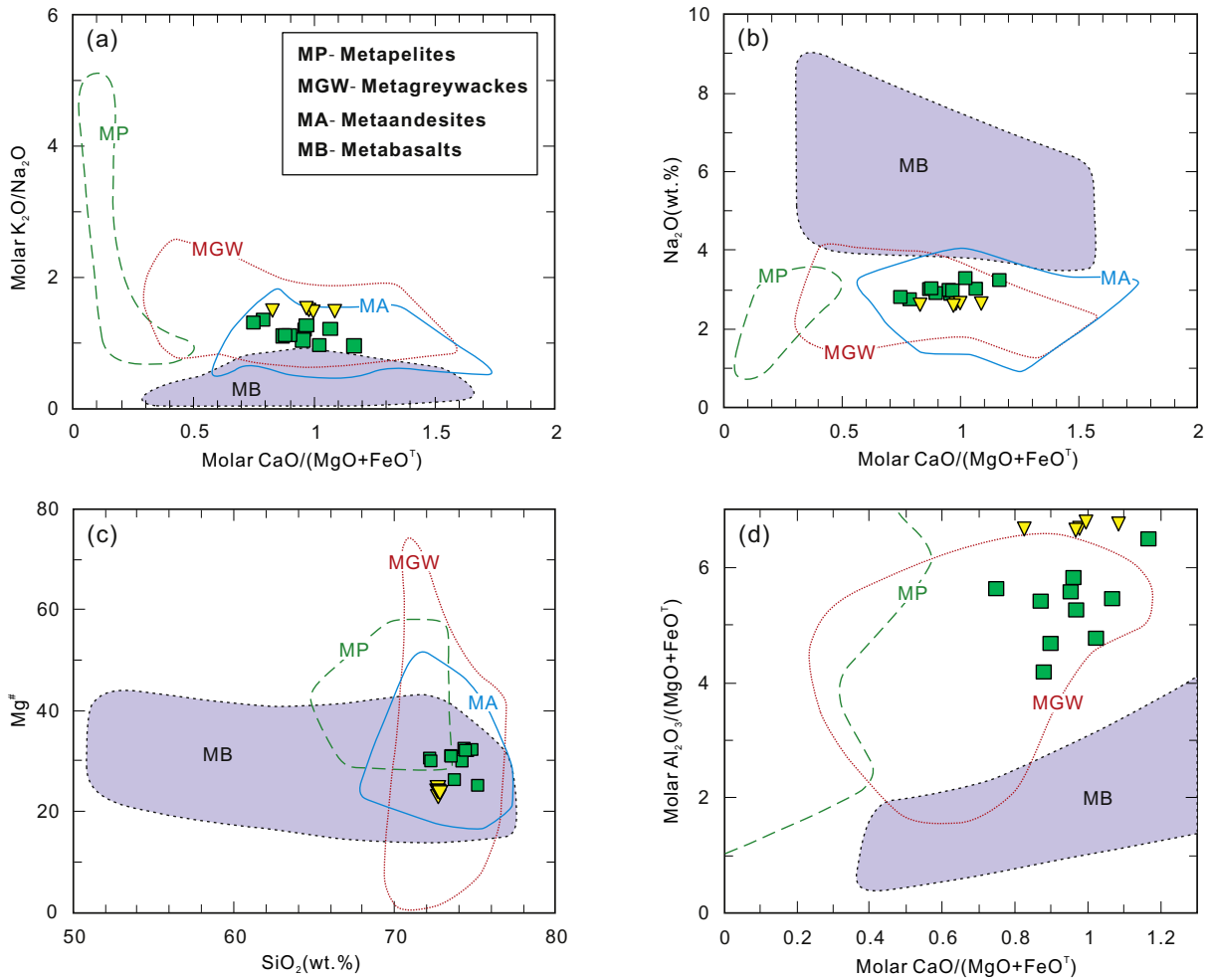
Fig. 9. Molar K$_2$O/Na$_2$O, Na$_2$O, and molar Al$_2$O$_3$/(MgO + FeO^T) versus molar CaO/(MgO + FeO^T) (a–b, d) and Mg$^\#$ versus SiO$_2$ (c) diagrams showing compositions of the Huolushan and Longyandong two-mica granites, together with compositional ranges of crustal melts (metagreywackes, metapelites, meta-andesites, and metabasalts) after Altherr et al. (2000) and Altherr and Siebel (2002). The legend is as in Fig. 5.
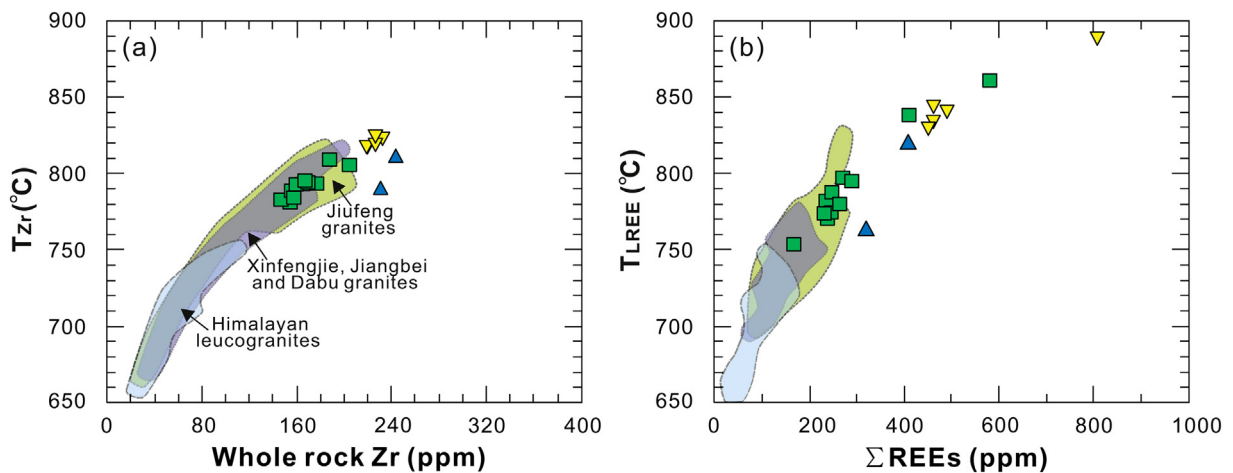

Fig. 10. (a) T$_{Zr}$ (zircon saturation temperature) versus whole-rock zirconium content diagram (Watson and Harrison, 1983) and (b) T$_{LREE}$ (monazite saturation temperature) versus ∑REE diagram (Montel, 1993) for the Huolushan two-mica granites and syenite porphyries and the Longyandong two-mica granites. Data sources and legend are as in Fig. 5.

assuming a magma temperature of 700 °C. The Huolushan two-mica granites have zircon saturation temperatures of 781–809 °C (Fig. 10a; Supplementary Table 7). Furthermore, an experimental study of leucogranites has suggested that primary muscovite can crystallize at

~700 °C (Huang et al., 2015a, and references therein). Therefore, it is reasonable to estimate the formation pressure of muscovite using a temperature of 700 °C. Moreover, the intrusion depth of the Huolushan two-mica granites can be estimated because the granites were intruded

by the younger diorites. Amphiboles in the Huolushan diorites are suitable for application of the Al-in-amphibole barometer given that they have a Ti content of <0.15 (cations per 23 oxygens) (Schmidt, 1992). The result of the calculation indicates that amphiboles in the Huolushan diorites crystallized at 1.8 ± 0.1 (1SD) kbar (Putirka, 2016; Supplementary Table 6), corresponding to a depth of ~6 km assuming a pressure gradient of ~3.3 km/kbar. In summary, the magma that formed the Huolushan two-mica granites was generated within the middle crust (16.5–20 km), following which the magma ascended and was finally emplaced within the upper crust (~6 km).

4.1.2. Fractional crystallization

The Huolushan granites may have undergone fractional crystallization of biotite, plagioclase, titanite, ilmenite, and apatite, based on the following lines of evidence. In a Harker diagram, the gradual decreases in TiO_2 and P_2O_5 contents with increasing SiO_2 content reflect separation of Ti-bearing minerals such as ilmenite and titanite and of P-bearing minerals such as apatite, respectively (Supplementary Fig. 4b, g). Furthermore, the gradual decreases in Al_2O_3, $Fe_2O_3^T$, and CaO contents with increasing SiO_2 content (Supplementary Fig. 4a, c, e) indicate separation of biotite and plagioclase, which are enriched in these elements. Moreover, plagioclase rims have markedly lower An values (16–21) than those of core domains (28–33), also suggesting fractional crystallization of plagioclase (Fig. 2m; Supplementary Table 2).

4.2. Huolushan syenite porphyries

Based on the geochemical and isotopic evidence described below, we suggest that the Huolushan syenite porphyries were formed by mixing of alkaline magmas derived from enriched mantle with felsic magmas derived from basement metasedimentary rocks of the Cathaysia Block. The Huolushan syenite porphyries have similar major- and trace-element characteristics to Jurassic (ca. 160 Ma) syenites that crop out in Guangxi and Jiangxi provinces (Figs. 5 and 6). The Jurassic syenites in the SCB have been suggested to be derived from enriched lithospheric mantle sources that were metasomatized by OIB-type melts (Li et al., 2003, 2004) or formed by mixing of asthenosphere-derived magmas with melts from enriched lithospheric mantle (He et al., 2010), plus variable degrees of fractional crystallization and crustal contamination. However, the Huolushan syenite porphyries, compared with the Guangxi and Jiangxi Jurassic syenites, have markedly lower Nb/Y ratios (0.63–0.97 and 1.1–6.2, respectively), more pronounced negative Eu anomalies (Eu/Eu* = 0.37–0.38 and 0.50–1.86, respectively), and more enriched Sr—Nd isotopic compositions (($^{87}Sr/^{86}Sr)_i$ = 0.7105–0.7119 and $\varepsilon_{Nd}(t)$ = −9.9 to −9.8, and ($^{87}Sr/^{86}Sr)_i$ = 0.7028–0.7098 and $\varepsilon_{Nd}(t)$ = −4.1 to +5.5, respectively) (Supplementary Tables S7–8; Fig. 7a; Li et al., 2004; He et al., 2010). The Sr—Nd isotopic compositions of the Huolushan syenite porphyries fall within the field of Triassic syenites and mafic shoshonitic rocks in the SCB that were derived from enriched lithospheric mantle (($^{87}Sr/^{86}Sr)_i$ = 0.7078–0.7123 and $\varepsilon_{Nd}(t)$ = −10.6 to −4.9; Wang et al., 2005; Mao et al., 2013a; Jiang et al., 2015). Compared with these Triassic syenites and mafic rocks, the Huolushan syenite porphyries do not contain aegirine or augite (Fig. 2i–j). In addition, the Huolushan syenite porphyries have lower MgO contents (0.67–0.81 wt%) than those of most of the Triassic syenites and mafic rocks mentioned above (0.23–6.27 wt%) (Supplementary Table 7). Therefore, the magma source of the Huolushan syenite porphyries was different from that of Triassic and Jurassic syenites and mafic shoshonitic rocks of the SCB. The Huolushan syenite porphyries show similar REE- and trace-element-variation patterns to those of the Huolushan two-mica granites (Fig. 6c–d). Most of the zircons from the syenite porphyries have similar $\delta^{18}O$ values (8.0‰–10.6‰, except for three with 6.5‰–7.8‰) to those of sedimentary-rock-derived granites (Fig. 8; Supplementary Fig. 6e; Supplementary Table 9). These geochemical features suggest that the

source material of the Huolushan syenite porphyries was derived predominantly from crustal sedimentary rocks. In addition, zircons of the Huolushan syenite porphyries also show a wide range of initial $^{176}Hf/^{177}Hf$ ratios of 0.282273–0.282505 with $\varepsilon_{Hf}(t)$ values ranging from −14.1 to −5.9 (Fig. 7b; Supplementary Fig. 5e; Supplementary Table 9). In a zircon Hf—O isotopic diagram, zircon $\varepsilon_{Hf}(t)$ values of syenite porphyries show a negative relationship with $\delta^{18}O$ values (Fig. 8). Furthermore, several oval mafic magmatic enclaves are observed in the Huolushan two-mica granites (Supplementary Fig. 3a–c) and may have been generated by mixing between coeval mafic magmas and two-mica granitic magmas in this area. Given that the Huolushan syenite porphyries are coeval with the Huolushan two-mica granites, they most probably formed by mixing of alkaline magmas derived from enriched mantle with felsic magmas derived from basement metasedimentary rocks of the Cathaysia Block (Fig. 7a).

The proportions of mantle- and crustal-derived melts that were involved in generating the Huolushan syenite porphyries can be further constrained using Sr—Nd isotopic modeling. The modeling curve used the Jurassic Xinfengjie biotite granite of the SCB as the crustal-sediment component and the Jurassic Qinghu syenite as the mantle end-member. The Jurassic (ca. 149 Ma) Xinfengjie granites are located within central Jiangxi Province and are regarded as S-type granites generated by melting of basement metasedimentary rocks of the Cathaysia Block (Jiang and Zhu, 2017). The Qinghu syenites could represent late Mesozoic primary syenitic magmas with little or no crustal contamination (Li et al., 2004). The Sr—Nd isotopic modeling results indicate that the Huolushan syenite porphyries can be produced by 10%–15% enriched-mantle-derived alkaline magmas mixing with 85%–90% metasedimentary-rock-derived felsic magmas (Fig. 7a).

4.3. Huolushan diorites

The Huolushan diorites have intermediate SiO_2 contents (SiO_2 = 59.9–60.4 wt%) and are metaluminous (A/CNK = 0.87) and calc-alkaline. In general, calc-alkaline intermediate magmatic rocks may be generated by three mechanisms: (1) direct melting of lower-crust mafic rock, (2) fractional crystallization of mantle-derived mafic magma, and (3) magma mixing (Tang et al., 2017, and references therein). Typically, magma mixing between mafic magma and felsic magma should result in negative relationships between whole-rock Sr and Nd isotopes and between zircon Hf and O isotopes (Li et al., 2009b). The Huolushan diorites have homogeneous Sr—Nd isotopic compositions (Fig. 7a; Supplementary Table 8) and also exhibit a rough positive trend in a zircon Hf—O isotope diagram (Supplementary Fig. 8). Therefore, it is inferred that the Huolushan diorites were not generated by magma mixing.

The Huolushan diorites have low MgO contents (2.86–2.90 wt%). They also have more enriched Sr—Nd isotopic compositions (($^{87}Sr/^{86}Sr)_i$ = 0.7106–0.7109; $\varepsilon_{Nd}(t)$ = −8.8 to −8.6) compared with Middle Jurassic within-plate basalts and gabbros of the Cathaysia Block (Fig. 7a). Moreover, the diorites have higher zircon $\delta^{18}O$ values (7.8‰–8.9‰) than those of mantle-derived Qinghu syenites ($\delta^{18}O$ = 5.4‰; Li et al., 2009b) and Yangchun basin granites that were derived from partial melting of basaltic rocks ($\delta^{18}O$ = 6.3‰–7.9‰; Huang et al., 2013). Therefore, the Huolushan diorites may have been generated by crustal assimilation and fractional crystallization (AFC) of mafic magmas derived from the mantle or of magmas derived from lower-crustal mafic rocks. In general, mantle-derived mafic rocks have low SiO_2 contents (<52 wt%; Jiang et al., 2009). Given that the Huolushan diorites have higher SiO_2 contents (59.9–60.4 wt%) than the mafic rocks (Supplementary Table 7), fractional crystallization of mafic magmas would involve separation of mafic minerals such as olivine and pyroxene. However, the Huolushan diorites do not contain the mafic minerals that commonly crystallize in mantle-derived mafic magmas (Fig. 2g and h). Therefore, the primary magmas of the Huolushan diorites were unlikely to have been derived from the mantle.

Some Mesozoic intermediate magmatic rocks have been inferred to be AFC products of primary magmas that were derived from lower-crustal granulite xenoliths from Cenozoic basalts in the SCB (Yu et al., 2003). The protoliths of those lower-crustal granulite xenoliths have been suggested to be underplated continental-arc-type basaltic rocks (Yu et al., 2003). Therefore, we suggest that the Huolushan diorites are more likely to have been generated by AFC processes in magmas derived from lower-crustal mafic rocks, given that the Huolushan diorites are characterized by Nb and Ta depletion (Fig. 6d) and have similar Sr—Nd isotopic compositions to those of lower-crust granulite xenoliths (Fig. 7a).

4.4. Longyandong two-mica granites

Whole-rock major- and trace-element characteristics and whole-rock Sr—Nd and zircon Hf—O isotopic compositions suggest that the Longyandong two-mica granites were formed by partial melting of metagreywackes. The Longyandong two-mica granites have similar major- and trace-element characteristics to those of sedimentary-rock-derived Himalayan leucogranites, Jiufeng two-mica granites, and Xinfengjie, Jiangbei, and Dabu biotite granites and muscovite-bearing granites in the SCB (Figs. 5 and 6). In particular, their Th contents and Th/La ratios (59.0–61.8 ppm and 0.31–0.54, respectively; Supplementary Table 7) are similar to or higher than those of the above-mentioned sedimentary-rock-derived granites (1.35–46.3 ppm and 0.23–3.0, respectively) (Guo and Wilson, 2012; Huang et al., 2015a; Jiang and Zhu, 2017). In addition, whole-rock Sr—Nd and zircon Hf isotopic compositions (($^{87}Sr/^{86}Sr)_i$ = 0.7094–0.7095, $\varepsilon_{Nd}(t)$ = −9.4 to −9.3, and $\varepsilon_{Hf}(t)$ = −12.3 to −4.9) of the Longyandong two-mica granites are similar to those of basement metasedimentary rocks of the Cathaysia Block, Triassic and Jurassic S-type granites of the SCB, and Himalayan leucogranites (Fig. 7a and b; Supplementary Tables 8–9). Moreover, the Longyandong two-mica granites show zircon $\delta^{18}O$ values (8.6‰–9.9‰; Supplementary Fig. 6f; Supplementary Table 9) that are similar to those of sedimentary-rock-derived Himalayan leucogranites, Neoproterozoic Jiuling S-type granites, Triassic Darongshan cordierite-bearing granites, and Jurassic Jiuyishan A-type granites in the SCB ($\delta^{18}O$ = 8.2‰–12.9‰; Fig. 8). Therefore, the source material of the Longyandong two-mica granites is inferred to have been basement metasedimentary rocks of the Cathaysia Block. Similar to the Huolushan two-mica granites, moderate molar $CaO/(MgO + FeO^T)$ and high molar $Al_2O_3/(MgO + FeO^T)$ ratios further indicate that the source metasedimentary rocks of the Longyandong two-mica granites were metagreywackes (Fig. 9).

Geochemical characteristics suggest that the Longyandong two-mica granites were formed by partial melting of metagreywackes, driven by dehydration melting of mica (muscovite or biotite) at crustal depths of >20 km. The Longyandong two-mica granites are characterized by higher K_2O (5.98–6.08 wt%) than Na_2O (2.61–2.68 wt%) contents (Supplementary Table 7). In addition, the Longyandong two-mica granites have high zircon (817–824 °C) and monazite (830–889 °C) saturation temperatures (Fig. 10a–b; Supplementary Table 7), which argues against water-saturated melting of plagioclase. The Longyandong two-mica granites have Sr—Nd isotopic compositions (($^{87}Sr/^{86}Sr)_i$ = 0.7094–0.7095, $\varepsilon_{Nd}(t)$ = −9.4 to −9.3) that are more depleted than those of the Huolushan two-mica granites (($^{87}Sr/^{86}Sr)_i$ = 0.7130–0.7145, $\varepsilon_{Nd}(t)$ = −10.5 to −10.2; Fig. 7a), meaning that their crustal sources differed. The higher La/Yb ratios (22.3–30.6, mean = 26.3) of the Longyandong two-mica granites relative to the Huolushan two-mica granites (15.3–29.5, mean = 22.3) (Supplementary Fig. 7b) suggest that the magma that formed the Longyandong two-mica granites originated at a greater depth than that of the Huolushan two-mica granites (~20 km, 6 kbar).

4.5. Geodynamic processes and implications

An extensional setting in southeastern China is indicated by the Early Jurassic (ca. 175 Ma) to Cenozoic rift at the eastern margin of China (Gilder et al., 1991), late Mesozoic extensional basins (Zhou et al., 2006; Zhou and Li, 2000), late Mesozoic metamorphic core complexes (Wang et al., 2006, and references therein), and late Mesozoic magmatism associated with crustal extension (A-type granites, syenites, OIB-type mafic rocks, and bimodal volcanic rocks; Liu et al., 2016; Zheng et al., 2017, and references therein; Yan and Jiang, 2019, and references therein; Wu et al., 2020). In addition, the Huolushan two-mica granites and syenite porphyries, and the Longyandong two-mica granites yield zircon (781–824 °C) and monazite (753–888 °C) saturation temperatures (Supplementary Table 7; Fig. 10a–b) that are markedly higher than those of most Himalayan leucogranites, the Xinfengjie, Jiangbei, and Dabu granites, and the Jiufeng granites in the SCB (Fig. 10a–b). Therefore, the relatively high magma temperatures of the Huolushan and Longyandong intrusive rocks suggest that underplating mafic magmas related to lithospheric extension may have acted as a key heat source and possibly also provided some material for their generation. Overall, the regional geological and geochemical evidence overwhelmingly indicates that the Huolushan two-mica granites and syenite porphyries and the Longyandong two-mica granites were formed in an extensional setting.

The tectonic environment of southeastern China during the Late Jurassic is generally considered to have been extensional (e.g., Huang et al., 2013, 2015a; Jiang et al., 2009; Li et al., 2007; Zhou et al., 2006). However, the mechanism for this extensional setting remains unresolved. Some studies have attributed the extension to reactivation of pre-existing fault/rift systems (He et al., 2010; Zhou et al., 2006) or delamination of a partially over-thickened lithospheric keel after the Triassic collision between Indochina and the SCB (Wang et al., 2013a). Others have suggested that lithospheric extension in a continental-arc setting was related to low-angle subduction of the Paleo-Pacific plate (Zhou and Li, 2000), in a back-/intra-arc setting was related to slab roll-back after normal subduction of the Paleo-Pacific plate (Jiang et al., 2009, 2015), or in an intraplate setting was a response to delamination of a flat-subducted Paleo-Pacific oceanic slab (Li et al., 2007; Li et al., 2018; Li and Li, 2007). Meng et al. (2012) compiled geochronological and geochemical data of typical Mesozoic basaltic rocks in the central-eastern SCB. These data reveal three evolutionary stages for these basalts: Early–early Late Jurassic (195 to 160 Ma), Late Jurassic– late Early Cretaceous (160 to 110 Ma), and late Early Cretaceous–Early Paleocene (110 to 63 Ma), which could be explained by delamination and foundering of a flat-subducted Paleo-Pacific slab (Huang et al., 2013, 2015a; Meng et al., 2012). In addition, the late Early to earliest Middle Jurassic (ca. 180 to 173 Ma) crustal shorting revealed by seismic reflection data and widespread early Middle Jurassic to Early Cretaceous (ca. 172 to 118 Ma) magmatism across the SCB are inferred to have been associated with flat subduction of the Paleo-Pacific slab and subsequent slab foundering (Li et al., 2018). Moreover, ca. 160 Ma granites and syenites are widespread in southeastern China in both inland and coastal areas, and show intraplate geochemical characteristics (Fig. 1b; Li et al., 2007; Huang et al., 2013, 2015a; Li et al., 2018). Given that the Huolushan–Longyandong intrusive rocks were formed at 162 to 155 Ma (Fig. 3), they were probably generated in an intraplate extensional setting that developed in response to Late Jurassic delamination and foundering of the flat Paleo-Pacific slab. Underplating of mantle-derived magmas caused by a foundering slab would have provided most of the heat and some of the material required for the widespread Jurassic granitic magmatism.

A petrogenetic model for the Huolushan two-mica granites, diorites, and syenite porphyries and the Longyandong two-mica granites is presented in Fig. 11a–b. The Huolushan two-mica granites were most probably generated through fractional crystallization of magmas derived by
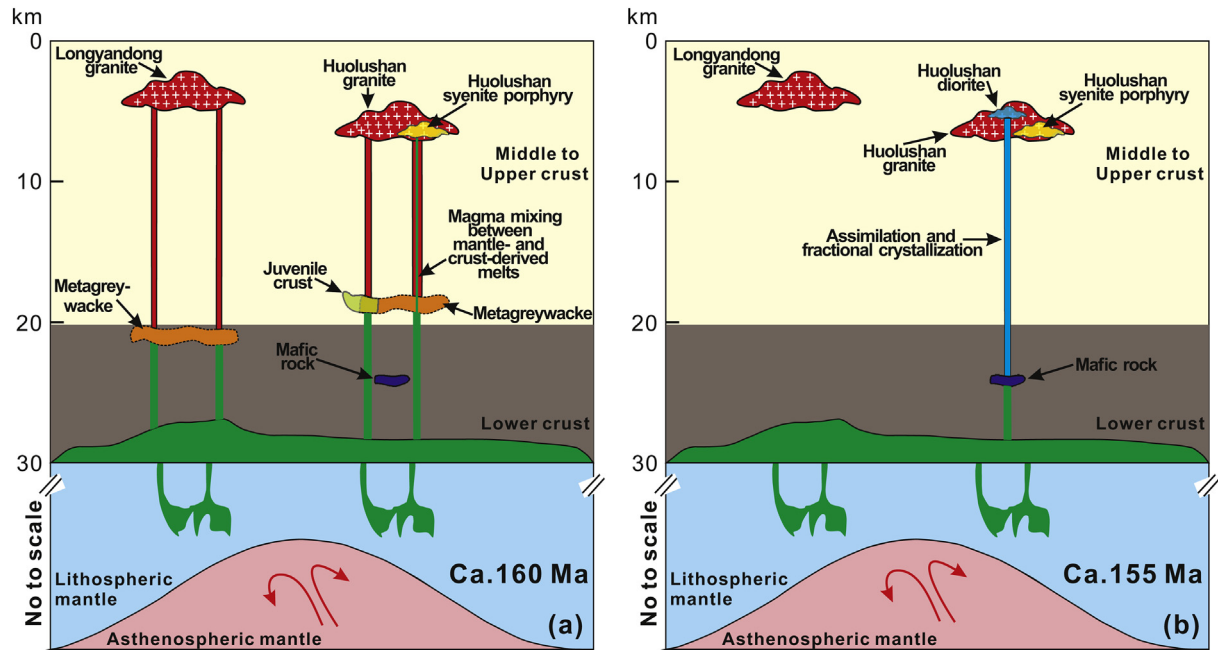
Fig. 11. Petrogenetic model for the Huolushan two-mica granites, diorites, and syenite porphyries and the Longyandong two-mica granites. (a) Lithospheric extension possibly related to delamination of a flat-subducted oceanic slab caused enriched-mantle-derived mafic magmas to be intruded into the middle to lower crust. Heat from the mafic magmas caused partial melting of the overlying metagreywackes and juvenile crust material. The Huolushan two-mica granites were formed by fractional crystallization of magmas that were derived from partial melting of a hybridized source consisting of metagreywackes with minor juvenile crustal rocks. The Huolushan syenite porphyries were generated by magma mixing between felsic magmas derived from metasedimentary rocks of the Cathaysia Block basement and minor enriched-mantle-derived alkaline magmas. The Longyandong two-mica granites were produced by partial melting of metagreywackes. (b) The Huolushan diorites were formed by assimilation and fractional crystallization of magmas that were derived from partial melting of lower-crust mafic rocks heated by mantle-derived mafic magmas.

partial melting of a hybridized source consisting of metagreywackes with minor juvenile crustal rocks. The magmas originated from depths of 16.5–20 km, which corresponds to the middle crust of the Cathaysia Block (Fig. 11a). Finally, the magmas were emplaced within the upper crust (~6 km) (Fig. 11a–b). The Huolushan syenite porphyries were formed by magmas derived from basement metasedimentary rocks mixing with minor (10%–15%) alkaline magmas derived from enriched lithospheric mantle of the Cathaysia Block (Fig. 11a). The Huolushan diorites were most likely formed by AFC processes in lower-crustal mafic-rock-derived magmas (Fig. 11b). The Longyandong two-mica granites were formed by partial melting of a middle- to lower-crust (>20 km) metagreywacke source (Fig. 11a–b).

Reworking and growth of continental crust are important topics of investigation in the field of continental dynamics (Zheng et al., 2007). Widespread Jurassic and Cretaceous granitoids indicate that continental crust of the SCB underwent significant reworking during the late Mesozoic (Huang et al., 2015a; Zhou et al., 2006; Zhou and Li, 2000). Our study suggests that the Huolushan and Longyandong two-mica granites were formed by reworking of middle- to lower-crustal metasedimentary rocks with subordinate juvenile crustal rocks heated by underplating mantle-derived mafic magmas. The Huolushan diorites were formed by reworking of lower-crustal mafic rocks heated by underplating mantle-derived mafic magmas, and these dioritic magmas underwent AFC during ascent. Therefore, both the middle and lower crust of the SCB underwent reworking during the late Mesozoic. Our study shows that reworking of middle crust of the SCB could have been induced by heating from mantle-derived mafic magmas in addition to in situ radiogenic heating related to over-thickened crust (Shu et al., 2015; Wang et al., 2007b). The formation of the Huolushan syenite porphyries was a result of crust–mantle interaction via magma mixing. Therefore, in addition to providing heat for late Mesozoic reworking of the SCB continental crust, mantle-derived mafic magmas also contributed to vertical crustal growth.

5. Conclusions

(1) SIMS zircon U—Pb dating results indicate that two-mica granites and associated diorites and syenite porphyries in the Huolushan–Longyandong area were formed during the Late Jurassic (162–155 Ma).

(2) The Huolushan granites were generated by fractional crystallization of magmas that were derived by partial melting of a hybridized source consisting of metagreywackes with minor juvenile crustal rocks. The Huolushan syenite porphyries were generated from mixing of felsic magmas derived from basement metasedimentary rocks of the Cathaysia Block with minor alkaline magmas derived from enriched mantle. The Huolushan diorites were most likely formed by partial melting of lower-crustal mafic rocks, and these dioritic magmas underwent AFC during ascent. The Longyandong two-mica granites were generated by partial melting of metagreywackes.

(3) Continental crust of the SCB underwent significant reworking during the late Mesozoic, involving middle- to lower-crustal metasedimentary rocks and juvenile crustal rocks as well as lower-crustal mafic rocks. In addition to supplying heat for reworking of the SCB, mantle-derived magmas also provided materials for late Mesozoic vertical crustal growth.

Supplementary data to this article can be found online at https://doi.org/10.1016/j.lithos.2020.105537.

Declaration of Competing Interest

The authors declare that they have no known competing financial interests or personal relationships that could have appeared to influence the work reported in this paper.

Acknowledgments

References

Altherr, R., Siebel, W., 2002. I-type plutonism in a continental back-arc setting: miocene granitoids and monzonites from the central Aegean Sea, Greece. Contrib. Mineral. Petrol. 143, 397–415.

Altherr, R., Holl, A., Hegner, E., Langer, C., Kreuzer, H., 2000. High-potassium, calc-alkaline I-type plutonism in the European Variscides: northern Vosges (France) and northern Schwarzwald (Germany). Lithos 50, 51–73.

Cawood, P.A., Kröner, A., Collins, W.J., Kusky, T.M., Mooney, W.D., Windley, B.F., 2009. Accretionary orogens through Earth history. Geol. Soc. Lond. Spec. Publ. 318, 1–36.

Chen, J.F., Jahn, B.M., 1998. Crustal evolution of southeastern China: Nd and Sr isotopic evidence. Tectonophysics 284, 101–133.

Chen, J.Y., Yang, J.H., Ji, W.Q., 2017. Ages and petrogenesis of Jurassic and cretaceous intrusive rocks in the Matsu Islands: implications for lower crust modification beneath southeastern China. J. Asian Earth Sci. 150, 14–24.

Chu, Y., Lin, W., Faure, M., Xue, Z.H., Ji, W.B., Feng, Z.T., 2019. Cretaceous episodic extension in the South China Block, East Asia: evidence from the Yuechengling Massif of Central South China. Tectonics 38, 3675–3702.

Gao, L.E., Zeng, L.S., 2014. Fluxed melting of metapelite and the formation of Miocene high-CaO two-mica granites in the Malashan gneiss dome, southern Tibet. Geochim. Cosmochim. Acta 130, 136–155.

Gao, P., Zhao, Z.F., Zheng, Y.F., 2014. Petrogenesis of Triassic granites from the Nanling Range in South China: implications for geochemical diversity in granites. Lithos 210–211, 40–56.

GDGBMR (Bureau of Geology and Mineral Resources of Guangdong Province), 1988. Regional Geology of Guangdong Province. Geological Publishing House, Beijing, pp. 1–941 (in Chinese).

Gilder, S.A., Keller, G.R., Luo, M., Goodell, P.C., 1991. Eastern Asia and the western Pacific timing and spatial distribution of rifting in China. Tectonophysics 197, 225–243.

Guo, Z.F., Wilson, M., 2012. The Himalayan leucogranites: constraints on the nature of their crustal source region and geodynamic setting. Gondwana Res. 22, 360–376.

Guo, X.F., Tian, Y., Zhang, X.B., 2019. Geochronology, genesis and landscape of Yanshanian granite in Guangzhou area, central Guangdong Province of China. SN Appl. Sci. 1, 1–11.

Hawthorne, F.C., 1981. Crystal chemistry of the amphiboles. Rev. Mineral. Geochem. 9A, 1–102.

He, Z.Y., Xu, X.S., Niu, Y.L., 2010. Petrogenesis and tectonic significance of a Mesozoic granite–syenite–gabbro association from inland South China. Lithos 119, 621–641.

Holdsworth, R.E., Handa, M., Miller, J.A., Buick, I.S., 2001. Continental reactivation and reworking: an introduction. Geol. Soc. Lond. Spec. Publ. 184, 1–12.

Hopkinson, T.N., Harris, N.B., Warren, C.J., Spencer, C.J., Roberts, N.M., Horstwood, M.S., Parrish, R.R., 2017. The identification and significance of pure sediment-derived granites. Earth Planet. Sci. Lett. 467, 57–63.

Hoskin, P., Black, L., 2000. Metamorphic zircon formation by solid-state recrystallization of protolith igneous zircon. J. Metamorph. Geol. 18, 423–439.

Huang, H.Q., Li, X.H., Li, W.X., Li, Z.X., 2011. Formation of high δ18O fayalite-bearing A-type granite by high-temperature melting of granulitic metasedimentary rocks, southern China. Geology 39, 903–906.

Huang, H.Q., Li, X.H., Li, Z.X., Li, W.X., 2013. Intraplate crustal remelting as the genesis of Jurassic high-K granites in the coastal region of the Guangdong Province, SE China. J. Asian Earth Sci. 74, 280–302.

Huang, H.Q., Li, X.H., Li, Z.X., Li, W.X., 2015a. Formation of the Jurassic South China Large Granitic Province: insights from the genesis of the Jiufeng pluton. Chem. Geol. 401, 43–58.

Huang, J.C., Peng, J.T., Yang, J.H., Zhang, B.L., Xu, C.X., 2015b. Precise zircon U-Pb and molybdenite Re-Os dating of the Shuikoushan granodiorite-related Pb-Zn mineralization, southern Hunan, South China. Ore Geol. Rev. 71, 305–317.

Huang, C.M., Zhao, Z.D., Li, G.M., Zhu, D.C., Liu, D., Shi, Q.S., 2017. Leucogranites in Lhozag, southern Tibet: implications for the tectonic evolution of the eastern Himalaya. Lithos 294–295, 246–262.

Jiang, Y.H., Zhu, S.Q., 2017. Petrogenesis of the Late Jurassic peraluminous biotite granites and muscovite-bearing granites in SE China: geochronological, elemental and Sr–Nd–O–Hf isotopic constraints. Contrib. Mineral. Petrol. 172, 1–27.

Jiang, Y.H., Jiang, S.Y., Dai, B.Z., Liao, S.Y., Zhao, K.D., Ling, H.F., 2009. Middle to late Jurassic felsic and mafic magmatism in southern Hunan province, southeast China: Implications for a continental arc to rifting. Lithos 107, 185–204.

Jiang, Y.H., Wang, G.C., Liu, Z., Ni, C.Y., Qing, L., Zhang, Q., 2015. Repeated slab advance–retreat of the Palaeo-Pacific plate underneath SE China. Int. Geol. Rev. 57, 472–491.

Jiao, S.J., Li, X.H., Huang, H.Q., Deng, X.G., 2015. Metasedimentary melting in the formation of charnockite: Petrological and zircon U-Pb-Hf-O isotope evidence from the Darongshan S-type granitic complex in southern China. Lithos 239, 217–233.

Li, Z.X., Li, X.H., 2007. Formation of the 1300-km-wide intracontinental orogen and postorogenic magmatic province in Mesozoic South China: a flat-slab subduction model. Geology 35, 179–182.

Li, X.H., Wang, Y.X., Zhao, Z.H., Chen, D.F., Zhang, H., 1998. SHRIMP U-Pb zircon geochronology for amphibolite from the Precambrian basement in SW Zhejiang and NW Fujian Province. Geochimica 27, 327–334 (in Chinese with English abstract).

Li, X.H., Chen, Z.G., Liu, D.Y., Li, W.X., 2003. Jurassic gabbro-granite-syenite suites from Southern Jiangxi Province, SE China: age, origin, and tectonic significance. Int. Geol. Rev. 45, 898–921.

Li, X.H., Chung, S.L., Zhou, H.W., Lo, C.H., Liu, Y., Chen, C.H., 2004. Jurassic intraplate magmatism in southern Hunan-eastern Guangxi: 40Ar/39Ar dating, geochemistry, Sr-Nd isotopes and implications for the tectonic evolution of SE China. Geol. Soc. Lond. Spec. Publ. 226, 193–215.

Li, W.X., Li, X.H., Li, Z.X., 2005. Neoproterozoic bimodal magmatism in the Cathaysia Block of South China and its tectonic significance. Precambrian Res. 136, 51–66.

Li, X.H., Li, Z.X., Li, W.X., Liu, Y., Yuan, C., Wei, G.J., Qi, C.S., 2007. U–Pb zircon, geochemical and Sr–Nd–Hf isotopic constraints on age and origin of Jurassic I- and A-type granites from central Guangdong, SE China: a major igneous event in response to foundering of a subducted flat-slab? Lithos 96, 186–204.

Li, X.H., Li, W.X., Li, Z.X., Lo, C.H., Wang, J., Ye, M.F., Yang, Y.H., 2009a. Amalgamation between the Yangtze and Cathaysia Blocks in South China: constraints from SHRIMP U–Pb zircon ages, geochemistry and Nd–Hf isotopes of the Shuangxiwu volcanic rocks. Precambrian Res. 174, 117–128.

Li, X.H., Li, W.X., Wang, X.C., Li, Q.L., Liu, Y., Tang, G.Q., 2009b. Role of mantle-derived magma in genesis of early Yanshanian granites in the Nanling Range, South China: in situ zircon Hf-O isotopic constraints. Sci. China Ser. D Earth Sci. 52, 1262–1278.

Li, Z.X., Li, X.H., Wartho, J.A., Clark, C., Li, W.X., Zhang, C.L., Bao, C., 2010. Magmatic and metamorphic events during the early Paleozoic Wuyi-Yunkai orogeny, southeastern South China: New age constraints and pressure-temperature conditions. Geol. Soc. Am. Bull. 122, 772–793.

Li, J.H., Dong, S.W., Cawood, P.A., Zhao, G.C., Johnston, S.T., Zhang, Y.Q., Xin, Y.J., 2018. An Andean-type retro-arc foreland system beneath northwest South China revealed by SINOPROBE profiling. Earth Planet. Sci. Lett. 490, 170–179.

Liu, L., Xu, X.S., Xia, Y., 2016. A synchronizing paleo-Pacific slab rollback beneath SE China: Insights from the episodic Late Mesozoic volcanism. Gondwana Res. 37, 397–407.

Liu, H.C., Wang, Y.J., Li, Z.H., Zi, J.W., Huangfu, P.P., 2018. Geodynamics of the Indosinian orogeny between the South China and Indochina blocks: insights from latest Permian–Triassic granitoids and numerical modeling. Geol. Soc. Am. Bull. 130, 1289–1306.

Mao, J.R., Ye, H.M., Liu, K., Li, Z.L., Takahashi, Y., Zhao, X.L., Kee, W.S., 2013a. The Indosinian collision–extension event between the South China Block and the Palaeo-Pacific plate: evidence from Indosinian alkaline granitic rocks in Dashuang, eastern Zhejiang, South China. Lithos 172-173, 81–97.

Mao, J.W., Cheng, Y.B., Chen, M.H., Pirajno, F., 2013b. Major types and time–space distribution of Mesozoic ore deposits in South China and their geodynamic settings. Miner. Deposita 48, 267–294.

Meng, L.F., Li, Z.X., Chen, H.L., Li, X.H., Wang, X.C., 2012. Geochronological and geochemical results from Mesozoic basalts in southern South China Block support the flat-slab subduction model. Lithos 132–133, 127–140.

Miller, C.F., Stoddard, E.F., Bradfish, L.J., Dollase, W.A., 1981. Composition of plutonic muscovite: genetic implications. Can. Mineral. 19, 25–34.

Montel, J.M., 1993. A model for monazite/melt equilibrium and application to the generation of granitic magmas. Chem. Geol. 110, 127–146.

O'Nions, R.K., Hamilton, P.J., Hooker, P.J., 1983. A Nd isotope investigation of sediments related to crustal development in the British Isles. Earth Planet. Sci. Lett. 63, 229–240.

Patiño Douce, A.E., Harris, N., 1998. Experimental constraints on Himalayan anatexis. J. Petrol. 39, 689–710.

Putirka, K., 2016. Amphibole thermometers and barometers for igneous systems and some implications for eruption mechanisms of felsic magmas at arc volcanoes. Am. Mineral. 101, 841–858.

Qi, C.S., Deng, X.G., Li, W.X., Li, X.H., Yang, Y.H., Xie, L.W., 2007. Origin of the Darongshan-Shiwandashan S-type granitoid belt from southeastern Guangxi: geochemical and Sr-Nd-Hf isotopic constraints. Acta Petrol. Sin. 23, 403–412 (in Chinese with English abstract).

Rong, W., Zhang, S.B., Zheng, Y.F., 2017. Back-reaction of peritectic garnet as an explanation for the origin of mafic enclaves in S-type granite from the Jiuling batholith in South China. J. Petrol. 58, 569–598.

Schmidt, M.W., 1992. Amphibole composition in tonalite as a function of pressure: an experimental calibration of the Al-in-hornblende barometer. Contrib. Mineral. Petrol. 110, 304–310.

Shen, W.Z., Ling, H.F., Li, W.X., Wang, D.Z., Huang, X., Pan, J., 1999. Nd-Sr isotopic study of Mesozoic granitoids in Jiangxi Province. Chin. Sci. Bull. 44, 1427–1431.

Shu, L.S., Wang, B., Cawood, P.A., Santosh, M., Xu, Z.Q., 2015. Early Paleozoic and Early Mesozoic intraplate tectonic and magmatic events in the Cathaysia Block, South China. Tectonics 34, 1600–1621.

Shu, L.S., Wang, J.Q., Yao, J.L., 2019. Tectonic evolution of the eastern Jiangnan region, South China: new findings and implications on the assembly of the Rodinia supercontinent. Precambrian Res. 322, 42–65.

Sun, T., 2006. A new map showing the distribution of granites in South China and its explanatory notes. Geol. Bull. China 25, 332–335 (in Chinese with English abstract).

Sun, S.S., McDonough, W.F., 1989. Chemical and isotopic systematics of oceanic basalts: Implications for mantle composition and processes. In: Saunders, A.D., Norry, M.J. (Eds.), Implications for Mantle Composition and Processes, Magmatism in the Ocean Basins. 42. Geological Society, London, pp. 313–345 (Special Publication).

Tang, G.J., Wang, Q., Zhang, C.F., Wyman, Derek A., Dan, W., Xia, X.P., Chen, H.Y., Zhao, Z.H., 2017. Sr-Nd-Hf-O isotope geochemistry of the Ertaibei pluton, East Junggar, NW China: Implications for development of a crustal-scale granitoid pluton and crustal growth. Geochem. Geophys. Geosyst. 18, 3340–3358.

Vernon, R.H., 2004. A Practical Guide to Rock Microstructure. Cambridge University Press, Cambridge, pp. 1–594.

Wang, Y.J., Fan, W.M., Guo, F., Peng, T.P., Li, C.W., 2003. Geochemistry of Mesozoic mafic rocks adjacent to the Chenzhou-Linwu fault, South China: implications for the lithospheric boundary between the Yangtze and Cathaysia blocks. Int. Geol. Rev. 45, 263–286.

Wang, Q., Li, J.W., Jian, P., Zhao, Z.H., Xiong, X.L., Bao, Z.W., Xu, J.F., Li, C.F., Ma, J.L., 2005. Alkaline syenites in eastern Cathaysia (South China): link to Permian–Triassic transtension. Earth Planet. Sci. Lett. 230, 339–354.

Wang, Q., Xu, J.F., Jian, P., Bao, Z.W., Zhao, Z.H., Li, C.F., Xiong, X.L., Ma, J.L., 2006. Petrogenesis of adakitic porphyries in an extensional tectonic setting, Dexing, South China: implications for the genesis of porphyry copper mineralization. J. Petrol. 47, 119–144.

Wang, Y.J., Fan, W.M., Cawood, P.A., Ji, S.C., Peng, T.P., Chen, X.Y., 2007a. Indosinian high-strain deformation for the Yunkaidashan tectonic belt, south China: kinematics and $^{40}Ar/^{39}Ar$ geochronological constraints. Tectonics 26, 1–21.

Wang, Y.J., Fan, W.M., Sun, M., Liang, X.Q., Zhang, Y.H., Peng, T.P., 2007b. Geochronological, geochemical and geothermal constraints on petrogenesis of the Indosinian peraluminous granites in the South China Block: a case study in the Hunan Province. Lithos 96, 475–502.

Wang, Y.J., Zhang, F.F., Fan, W.M., Zhang, G.W., Chen, S.Y., Cawood, P.A., Zhang, A.M., 2010. Tectonic setting of the South China Block in the early Paleozoic: resolving intracontinental and ocean closure models from detrital zircon U-Pb geochronology. Tectonics 29, 1–16.

Wang, Y.J., Fan, W.M., Zhang, G.W., Zhang, Y.H., 2013a. Phanerozoic tectonics of the South China Block: key observations and controversies. Gondwana Res. 23, 1273–1305.

Wang, Y.J., Zhang, A.M., Cawood, P.A., Fan, W.M., Xu, J.F., Zhang, G.W., Zhang, Y.Z., 2013b. Geochronological, geochemical and Nd–Hf–Os isotopic fingerprinting of an early Neoproterozoic arc–back-arc system in South China and its accretionary assembly along the margin of Rodinia. Precambrian Res. 231, 343–371.

Wang, G.C., Jiang, Y.H., Liu, Z., Ni, C.Y., Qing, L., Zhang, Q., Zhu, S.Q., 2016a. Multiple origins for the Middle Jurassic to Early Cretaceous high-K calc-alkaline I-type granites in northwestern Fujian province, SE China and tectonic implications. Lithos 246-247, 197–211.

Wang, Q., Hawkesworth, C.J., Wyman, D., Chung, S.L., Wu, F.Y., Li, X.H., Li, Z.X., Gou, G.N., Zhang, X.Z., Tang, G.J., Dan, W., Ma, L., Dong, Y.H., 2016b. Pliocene-Quaternary crustal melting in central and northern Tibet and insights into crustal flow. Nat. Commun. 7, 1–11.

Watson, E.B., Harrison, T.M., 1983. Zircon saturation revisited: temperature and composition effects in a variety of crustal magma types. Earth Planet. Sci. Lett. 64, 295–304.

Wu, Y.M., Guo, F., Wang, X.C., Wilde, S.A., Fan, W.M., 2020. Derivation of Jurassic HIMU-like intraplate basalts from mantle transition zone in South China: new geochemical constraints from olivine-hosted melt inclusion. Lithos 354–355, 1–14.

Yan, X., Jiang, S.Y., 2019. Petrogenesis and tectonic implications of Early Cretaceous shoshonitic syenites in the northern Wuyi Mt Range, Southeast China. J. Asian Earth Sci. 180, 1–20.

Yu, J.H., Xu, X.S., O'Reilly, S.Y., Griffin, W.L., Zhang, M., 2003. Granulite xenoliths from Cenozoic Basalts in SE China provide geochemical fingerprints to distinguish lower crust terranes from the North and South China tectonic blocks. Lithos 67, 77–102.

Yu, J.H., O'Reilly, S.Y., Zhou, M.F., Griffin, W.L., Wang, L.J., 2012. U–Pb geochronology and Hf–Nd isotopic geochemistry of the Badu Complex, Southeastern China: implications for the Precambrian crustal evolution and paleogeography of the Cathaysia Block. Precambrian Res. 222–223, 424–449.

Yu, Y., Huang, X.L., He, P.L., Li, J., 2016. I-type granitoids associated with the early Paleozoic intracontinental orogenic collapse along pre–existing block boundary in South China. Lithos 248, 353–365.

Yuan, Z.X., Wu, L.S., Zhang, Z.Q., Ye, X.J., 1991. The Sm-Nd, Rb-Sr isotopic age-dating of Mayuan group in northern Fujian. Acta Petrol. Mineral. 10, 127–132 (in Chinese with English abstract).

Zhang, Y., Yang, J.H., Sun, J.F., Zhang, J.H., Chen, J.Y., Li, X.H., 2015. Petrogenesis of Jurassic fractionated I-type granites in Southeast China: constraints from whole-rock geochemical and zircon U–Pb and Hf–O isotopes. J. Asian Earth Sci. 111, 268–283.

Zhao, G.C., 2015. Jiangnan Orogen in South China: developing from divergent double subduction. Gondwana Res. 27, 1173–1180.

Zhao, Z.F., Zheng, Y.F., 2009. Remelting of subducted continental lithosphere: Petrogenesis of Mesozoic magmatic rocks in the Dabie-Sulu orogenic belt. Sci. China Ser. D Earth Sci. 52, 1295–1318.

Zheng, Y.F., Zhang, S.B., Zhao, Z.F., Wu, Y.B., Li, X.H., Li, Z.X., Wu, F.Y., 2007. Contrasting zircon Hf and O isotopes in the two episodes of Neoproterozoic granitoids in South China: implications for growth and reworking of continental crust. Lithos 96, 127–150.

Zheng, W., Mao, J.W., Zhao, H.J., Zhao, C.S., Yu, X.F., 2017. Two Late Cretaceous A-type granites related to the Yingwuling W–Sn polymetallic mineralization in Guangdong province, South China: implications for petrogenesis, geodynamic setting, and mineralization. Lithos 274, 106–122.

Zhou, X.M., Li, W.X., 2000. Origin of Late Mesozoic igneous rocks in Southeastern China: implications for lithosphere subduction and underplating of mafic magmas. Tectonophysics 326, 269–287.

Zhou, X.M., Sun, T., Shen, W.Z., Shu, L.S., Niu, Y.L., 2006. Petrogenesis of Mesozoic granitoids and volcanic rocks in South China: a response to tectonic evolution. Episodes 29, 26–33.